Fryer, P., Pearce, J. A., Stokking, L. B., et al., 1990
Proceedings of the Ocean Drilling Program, Initial Reports, Vol. 125

7. SITE 779[1]

Shipboard Scientific Party[2]

HOLE 779A

Date occupied: 25 February 1989

Date departed: 7 days 3 hr 15 min

Position: 19°30.75′N, 146°41.75′E

Bottom felt (rig floor; m, drill-pipe measurement): 3957.9

Distance between rig floor and sea level (m): 10.7

Water depth (drill-pipe measurement from sea level, m): 3947.2

Total depth (rig floor, m): 4275.1

Penetration (m): 317.2

Number of cores: 37

Total length of cored section (m): 319.2

Total core recovered (m): 73.2

Core recovery (%): 22.9

Oldest sediment cored:
Depth (mbsf): 317.2
Nature: serpentine breccia
Earliest age: early Pliocene(?) to late Miocene(?)

Hard rock:
Nature: clasts(?) of serpentinized mafic and ultramafic rocks in a serpentine matrix

HOLE 779B

Date occupied: 28 February 1989

Date departed: 28 February 1989

Time on hole: 1 hr

Position: 19°30.75′N, 146°41.75′E

Bottom felt (rig floor; m, drill-pipe measurement): 3957.9

Distance between rig floor and sea level (m): 10.7

Water depth (drill-pipe measurement from sea level, m): 3947.2

Total depth (rig floor, m): 3966.9

Penetration (m): 9.0

Number of cores: 1

Total length of cored section (m): 9.0

Total core recovered (m): 8.7

Core recovery (%): 96.7

Oldest sediment cored:
Depth (mbsf): 8.7
Nature: silt-sized serpentine, serpentine silt, serpentine-rich silty sand
Earliest age: early Pleistocene

Principal results: Site 779 is situated about halfway up the southeast flank of Conical Seamount, approximately 3.5 km northeast of Site 778. Two holes were drilled: Hole 779A (which reached 317.2 mbsf) and Hole 779B (which was a single 9-m core aimed at recovering the uppermost sediment). Recovery at Hole 779A averaged 22.9%. As at Site 778, our principal aim was to penetrate serpentine flows on the flank of the seamount, to reach the underlying sediments, and if possible, basement in order to study the construction of the seamount, the origin and emplacement of the serpentine flows and serpentinites, and the nature and metamorphic history of forearc lithosphere. Three major lithostratigraphic units were recovered at Site 779:

1. Unit I (0–10.6 mbsf in Hole 779A and 0–9 mbsf in Hole 779B), comprising Holocene (?) to lower Pleistocene unconsolidated sediments and unconsolidated serpentine flows;
2. Unit II, comprising lower Pleistocene to lower Pliocene(?) or upper Miocene(?) sheared serpentine and subdivided into Subunit IIA (10.6–216.2 mbsf) and Subunit IIB (216.2–303.0 mbsf) on the basis of the absence and presence, respectively, of detrital serpentine sediments; and
3. Unit III (303.0–317.2 mbsf), comprising serpentine breccia with convolute layering.

The sheared serpentine is made up of clasts in a soft, serpentinized matrix. Clast lithologies are mostly of two types: (1) serpentinized, tectonized ultramafic rocks and (2) subordinate metabasic rocks. The ultramafic clasts are mostly harzburgite and subordinate dunite, with similar primary mineralogies to Hole 778A. The degree of serpentinization is variable, but shows an overall decrease downhole; serpentine veins are common and show a polystage filling history. Mafic clasts include both metabasalts and metagabbros, with primary mineralogies dominated by plagioclase and clinopyroxene in a glassy matrix (in basalts). Clay minerals, chlorite, pumpellyite, and, rarely, albite and sphene are the common metamorphic minerals. Structural studies show a complex history of deformation with no obvious relationship between the orientation of the clasts and matrix deformation. Gentle flowage under an applied load would explain the observed structures.

The serpentine-rich material in Subunit IIB contains recrystallized carbonate, kerogen(?), and filamentous aggregates of opaque minerals that may be bacterial remnants. The presence of kerogen indicates a primary sedimentary origin for this material, an interpretation supported by the presence of horizontal bedding within the same unit. Hydrocarbons increased dramatically with depth in Hole 779A, with methane, ethane, and propane present in most samples. A maximum of 30% methane was analyzed from one gas pocket sampled through the core liner. Analyses of interstitial pore-water samples at Site 779 show major variations from 0 to 100 mbsf in which pH increases to a maximum of 11.9, alkalinity increases five-fold, calcium decreases by 80%, both salinity and chlorinity decrease by 10%, and magnesium is totally depleted. These results confirm the presence of a fluid other than seawater, possibly from the subducting plate, as proposed for Site 778. The fluids differ sufficiently from those of Site 778 to indicate considerable lateral variation in interstitial water composition within the flank materials of the seamount.

BACKGROUND AND SCIENTIFIC OBJECTIVES

Site 779 is the second of a series of sites (Sites 778 through 780) on Conical Seamount, a roughly circular seamount having a basal diameter of about 20 km and a relief of

[1] Fryer, P., Pearce, J. A., Stokking, L. B., 1990. *Proc. ODP, Init. Repts.*, 125: College Station, TX (Ocean Drilling Program).
[2] Shipboard Scientific Party is as given in list of participants preceding the contents.

1500 m, which lies on the outer-arc high of the Mariana forearc at a distance of about 100 km from the trench axis (see "Introduction" chapter, this volume, and Fig. 1). The site was chosen to penetrate the flank of the seamount at about 4000 m in a region devoid of surficial serpentine flows (showing low backscatter on SeaMARC II side-scanning sonar imagery of the seamount) on the southeast flank of the seamount. Site 779 was located about 3.5 km to the east-northeast of the first site on the flank of the seamount. *Alvin* dives near this site suggested that the seamount in this area was mantled by a pelagic sediment cover, and in some places by a thin manganese pavement, overlying exposures of unconsolidated serpentine containing serpentinized clasts of mafic and ultramafic rocks (Fryer et al., 1985; Fryer et al., this volume). Fractures in the manganese pavement that mantles portions of the dive area showed that the region had experienced recent surficial deformation. SeaMARC II side-scanning sonar imagery (Hussong and Fryer, 1985) further suggested that the site is located within a region that has been deformed by local tectonism (Fig. 2). Small relief fractures (mainly concentric to the summit) and a series of long-wavelength (up to 1.5 km) concentric ridges can be seen on the lower flank of the seamount within the area chosen for the site.

The specific objectives of drilling this flank site differ from those of Site 778 only in logistical considerations; we hoped that a more stable hole could be obtained by drilling in a region of potentially thicker sediment cover on the southeast quadrant of the seamount. Thus, our scientific objectives were as follows:

1. To determine the internal stratigraphy and the history of extrusion and deformation of a forearc serpentinite seamount;
2. To investigate the mode of emplacement of serpentine flows;
3. To determine the nature, composition, and age of forearc lithosphere;
4. To study the chemical effects of serpentinization on the forearc lithosphere and its sedimentary cover; and
5. To examine the process of dewatering of subducted oceanic lithosphere at a nonaccretionary convergent plate margin.

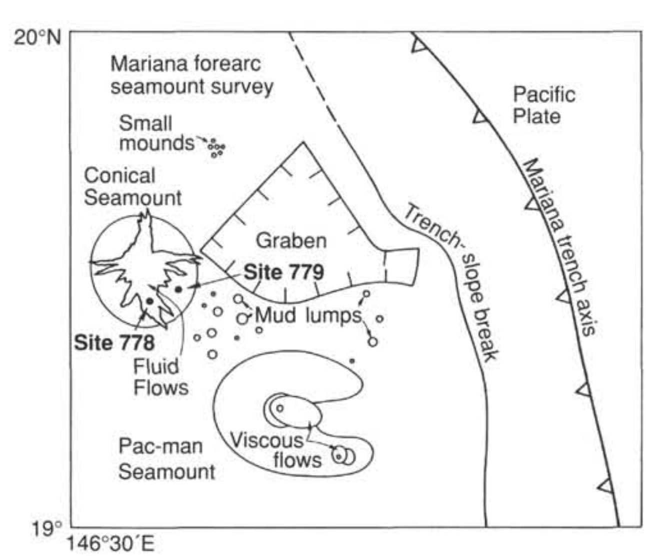

Figure 1. Schematic sketch of geologic features within the SeaMARC II survey area, including Conical Seamount and locations of Sites 778 and 779.

Because of the similarity in objectives between Sites 778 and 779, the same approach was adopted to achieve these objectives at the two sites (see "Background and Objectives" section, Site 778 chapter, this volume).

OPERATIONS

Site 779

Instead of offsetting and drilling another hole, it was proposed that we move around the flank of Conical Seamount to a location that appeared to contain less surface flow material. After obtaining official clearance, the drill string was pulled to 3479.3 m below sea level (bsl), and the ship was moved into the dynamic positioning mode (DP) 1.5 mi northeast to 19°30.75′N, 146°41.75′E. A beacon was dropped at 1400 hr UTC, 24 February, establishing Site 779.

Hole 779A

The drill string was lowered and Hole 779A was spudded at 1700UTC, 24 February. Water depth was established at 3947.2 m below sea level (bsl) by the first core. Hole problems began during the cutting of Core 125-779A-10R at 87.3 mbsf, after which a 20-bbl pill was pumped. Hole problems continued, and after Core 125-779A-11R, a short trip from 53 to 97 mbsf was made to improve the condition of the hole. After penetration to 170 mbsf, and after 51 hr of rotating time, the bit exhibited indications of failure. A free fall funnel (FFF) was dropped so that Hole 779A could be reentered after a round trip for a new bit.

The Colmec television camera was lowered in preparation for reentry. We found the FFF immediately, but owing to several rain squalls in the area, 1.5 hr was required for positioning the vessel before reentry, which we accomplished without incident. The television camera was retrieved and, after 3 hr of hole cleaning, the new bit was back at the previous total depth (TD).

Between taking Cores 125-779A-22R and 125-779A-23R (at a depth of 177.6 mbsf), the bottom of the hole caved in and 8 m of hole was lost. After 4 hr of reaming from 158 mbsf to bottom and pumping high-viscosity mud sweeps, coring resumed. The hole nevertheless required cleaning after each connection. Owing to the high risk to the drill string and logging tools, we did not consider it safe to log Hole 779A. However, we decided to continue coring the hole as long as possible, or until our time at the site expired.

The last 100 m of the hole provided few problems, and drilling continued to the end of our allotted site time. The RCB coring system was used to a TD of 317.2 mbsf, and we recovered 73.2 m of core in 37 deployments for a recovery rate of 23% (Table 1). Hole 779A and Site 779 ended at 1700UTC, 3 March, when the bit was back on deck and the vessel was under way.

Hole 779B

Before making the reentry into Hole 779A, a punch core of mud-line sediments was recovered that established Hole 779B at 2300UTC, 27 February. We retrieved the core barrel with 8.7 m of serpentine sediment for a recovery rate of 97% (Table 1).

LITHOSTRATIGRAPHY

Lithologic Summary

The stratigraphic section recovered at Site 779 has been divided into three lithologic units. Two subunits were assigned to lithologic Unit II, although this division may be artificial because of poor core recovery (having an average of only

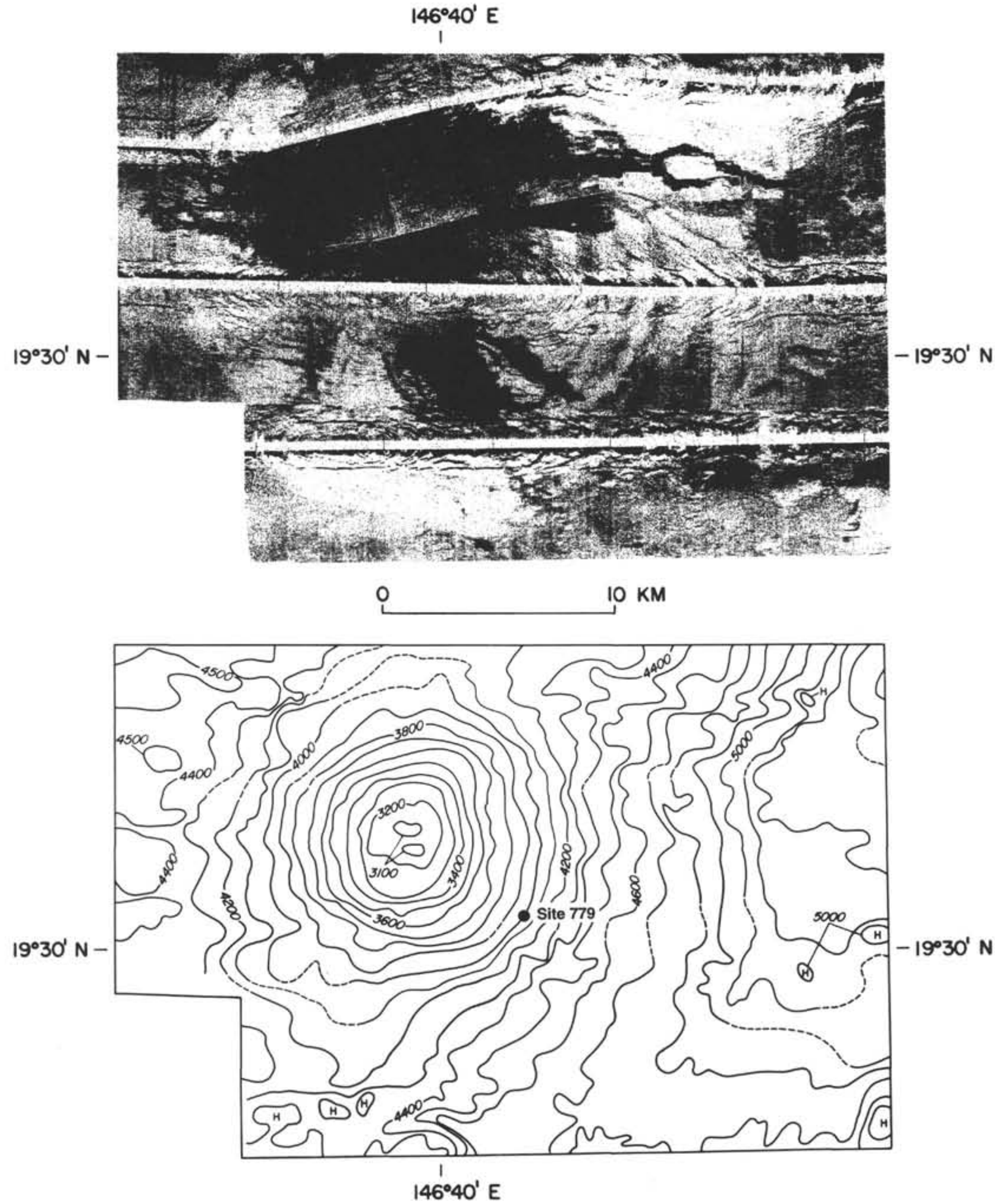

Figure 2. SeaMARC II side-scanning image of Conical Seamount (top), and SeaBeam bathymetric map of Conical Seamount showing Site 779 (bottom); bathymetry in meters.

23%, Table 1) and the possibility that unconsolidated matrix material and sediment were either washed away or created during the coring process. Lithologic Unit I consists of clay, silt-sized serpentine, and serpentine with clasts of serpentinized ultramafic rocks. Lithologic Subunit IIA is composed of blocks of serpentinized harzburgite and dunite, metabasalt, and serpentinite in a serpentine matrix. Lithologic Subunit IIB differs from lithologic Subunit IIA in that it has sediment intervals with distinct primary sedimentary and biologic structures. Lithologic Unit III is composed of serpentine microbreccia that has convolute layering. The units, their subbottom depths, lithologies, and biostratigraphic ages are summarized in Table 2.

Unit I

Hole 779A: Sections 125-779A-1R-1, 0 cm, to 125-779A-2R-5, 68 cm; depth, 0–10.6 mbsf.

Hole 779B: Sections 125-779B-1R-1, 0 cm, to 125-779B-1R-CC; depth, 0–9.0 mbsf.

Age: Holocene(?) to early Pleistocene.

This unit extends from the sediment/water interface to a total depth of 10.6 mbsf and primarily consists of serpentine clay and clayey silt-sized serpentine, with sand- to pebble-sized clasts of serpentinite and other lithic fragments. Of the strata recovered at this site, only Unit I contains sediment with well-preserved biogenic components. Some of the ser-

Table 1. Coring summary, Site 779.

Core no.	Date (1989)	Time (UTC)	Depth (mbsf)	Length cored (m)	Length recovered (m)	Recovery (%)
125-779A-1R	24 Feb.	1815	0–1.1	1.1	1.16	105.0
2R	24 Feb.	1935	1.1–10.6	9.5	6.70	70.5
3R	24 Feb.	2100	10.6–20.1	9.5	0.21	2.2
4R	25 Feb.	0015	20.1–29.6	9.5	0.50	5.3
5R	25 Feb.	0330	29.6–39.1	9.5	3.15	33.1
6R	25 Feb.	0540	39.1–48.5	9.4	0.44	4.7
7R	25 Feb.	0750	48.5–58.5	10.0	0.75	7.5
8R	25 Feb.	0955	58.5–68.1	9.6	0.75	7.8
9R	25 Feb.	1225	68.1–77.7	9.6	1.68	17.5
10R	25 Feb.	1510	77.7–87.3	9.6	1.88	19.6
11R	25 Feb.	1855	87.3–96.9	9.6	0.82	8.5
12R	26 Feb.	0045	96.9–106.6	9.7	0.62	6.4
13R	26 Feb.	0415	106.6–116.2	9.6	2.66	27.7
14R	26 Feb.	0700	116.2–125.9	9.7	2.67	27.5
15R	26 Feb.	0900	125.9–135.5	9.6	1.78	18.5
16R	26 Feb.	1250	135.5–145.2	9.7	2.53	26.1
17R	26 Feb.	1555	145.2–154.9	9.7	3.13	32.2
18R	26 Feb.	1905	154.9–159.4	4.5	3.08	68.4
19R	26 Feb.	2140	159.4–169.1	9.7	2.49	25.7
20R	27 Feb.	0045	169.1–170.1	1.0	0.77	77.0
21R	27 Feb.	0800	168.1–170.1	2.0	1.37	68.5
22R	28 Feb.	1150	170.1–177.6	7.5	3.15	42.0
23R	28 Feb.	1840	177.6–187.2	9.6	1.35	14.0
24R	1 March	0010	187.2–196.8	9.6	0.68	7.1
25R	1 March	0330	196.8–206.5	9.7	1.30	13.4
26R	1 March	0700	206.5–216.2	9.7	2.98	30.7
27R	1 March	0955	216.2–225.8	9.6	0.41	4.3
28R	1 March	1325	225.8–235.5	9.7	2.93	30.2
29R	1 March	1710	235.5–245.0	9.5	2.00	21.0
30R	1 March	2245	245.0–254.7	9.7	3.04	31.3
31R	2 March	0345	254.7–264.4	9.7	3.34	34.4
32R	2 March	0820	264.4–274.0	9.6	3.30	34.4
33R	2 March	1240	274.0–283.7	9.7	1.80	18.5
34R	2 March	1820	283.7–293.3	9.6	1.26	13.1
35R	2 March	200	293.3–303.0	9.7	1.34	13.8
36R	3 March	0245	303.0–312.7	9.7	3.43	35.3
37R	3 March	0610	312.7–317.2	4.5	1.79	39.8
Coring totals				319.2	73.24	22.9
125-779B-1R	27 Feb.	2345	0.0–9.0	9.0	8.70	96.6
	Coring Totals			9.0	8.70	96.6

pentine intervals within this unit lack biogenic and detrital components, but are underlain by sediment containing microfossils that indicate an early Pleistocene age, providing a maximum age for deposition of serpentine (see "Biostratigraphy" and "Paleomagnetism" sections, this chapter). On the basis of similar lithologies and biostratigraphic criteria, this unit correlates with Unit I at Site 778.

Brown (10YR 4/6 and 10YR 3/6) serpentine clay in the first core (Core 125-779A-1R) from Hole 779A is radiolarian-, nannofossil-, and foraminifer-bearing. The top of this core is 45 cm thick, soupy to moderately deformed, and artificially injected at Interval 125-779A-1R-1, 22 to 27 cm, with underlying light yellow (2.5Y 8/4) clayey silt-sized serpentine resulting from deformation. The brown serpentine clay contains clay minerals (40%), serpentine (32%), chlorite (5%), opaque minerals (3%), foraminifers (10%), nannofossils (5%), radiolarians (5%), and trace amounts of amphibole, lithic fragments, diatoms, and sponge spicules. The detrital material in the only core recovered from Hole 779B (100 m east of Hole 779A; see "Operations" section, this chapter) is a dark brown (10YR 3/3) serpentine silt and silty sand with trace amounts of radiolarians, silicoflagellates, nannofossils, and foraminifers. In Core 125-779B-1R, yellow to brownish-yellow (10YR 7/6 to 6/6), silt-sized serpentine is interlayered with soupy and moderately deformed dark-brown serpentine silt. The yellow silt-sized serpentine, found in the first cores from both Holes 779A and 779B, is stiff, very deformed, and lacks biogenic components. This silt-sized serpentine contains authigenic aragonite needles. The composition ranges from 60% to 75% serpentine, 7% to 20% opaque minerals, 0% to 15% aragonite, 5% to 10% zoisite, 0% to 5% clay minerals, 0% to a trace of chlorite, and 0% to a trace of garnet.

Core 125-779A-2R is composed of soupy to moderately deformed, aragonite-rich, sandy, silt-sized multicolored serpentine. In Section 125-779A-2R-1 at 56 to 77 cm, this sandy silt-sized serpentine is gray to very dark gray (2.5YR 5/0 to 3/0) with 70% serpentine, 20% aragonite, 5% opaque minerals, and 5% chlorite. The upper contact with the overlying yellow silt-sized serpentine found in the overlying core (125-779A-1R) was not recovered; there is a void in the core liner from 0 to 56 cm in Section 125-779A-2R-1. The lower contact of the gray sandy silt-sized serpentine is abrupt against a pale brown (10YR 7/4) serpentine with mottling of reddish-yellow (5YR 6/8) and light gray (7.5YR 7/0), sandy, silt-sized serpentine. This mottled lithology extends to the base of the unit. In composition, the light gray serpentine does not differ significantly from underlying mottled serpentine (62% to 70% serpentine, 15% to 20% aragonite, 5% to 10% opaque minerals, trace to 5% amphibole, and 0% to 5% zoisite and chlorite). Scattered black (7.5YR 2/0) and reddish-yellow (5YR 6/8) granule- to pebble-sized clasts of serpentinite or serpentinized ultramafic rocks are found throughout the serpentine of this unit.

Table 2. Lithologic units recovered at Site 779.

Lithologic unit/subunit	Cores	Depth (mbsf)	Dominant lithology	Stratigraphic age
I	125-779A-1R-1, 0 cm to 125-779A-2R-5, 68 cm; 125-779B-1R-1, 0 cm to 125-779B-1R-CC	0.0 to 10.6 0.0 to 9.0	Clay; silt-sized serpentine; lithic fragments in a matrix of sand- and silt-sized serpentine	Holocene(?) to lower Pleistocene
IIA	125-779A-3R-CC to 125-779A-26R-3, 150 cm	10.6 to 216.2	Blocks of serpentinized harzburgite and dunite, metabasalt, and serpentinite in a serpentine matrix	lower Pleistocene(?) to
IIB	125-779A-27R-1, 0 cm to 125-779A-35R-1, 133 cm	216.2 to 303.0	Blocks of gabbro, serpentinized harzburgite and dunite, and metabasalt, in a serpentine matrix with intercalations of detrital, fine-grained serpentine sediments	lower Pliocene(?)/ upper Miocene(?)
III	125-779A-36R-1, 0 cm to 125-779A-37R-CC	303.0 to 317.2	Serpentine breccia with convolute layering	(?)

Gray, sandy, silt-sized serpentine has been interpreted as a serpentine flow that extruded onto the seafloor under cool hydrothermal conditions because (1) the color is atypical of pelagic sediments in this area; (2) pelagic or detrital components are lacking; and (3) biological and sedimentological structures are absent. The gray color of the sandy, silt-sized serpentine may be the result of insufficient exposure to oxidizing conditions. In contrast, the yellowish-brown, pale brown, and reddish-brown of the overlying silt-sized serpentine suggest oxidation during prolonged exposure on the seafloor. On the basis of the second and third criteria, the yellowish-brown and pale brown silt-sized serpentines were also interpreted to represent serpentine flows. The reddish-brown and gray mottling in the pale brown silt-sized serpentine may represent mixing of previously oxidized and non-oxidized material (respectively) entrained during the extrusion. Alternatively, the mottling may be the result of drilling disturbance that mixed several layers of different oxidation states.

The yellowish-brown silt-sized serpentine from Core 125-779A-1R was deposited during or after the late middle Pleistocene, because it overlies sediment with nannofossils of this age from the core catcher (see "Biostratigraphy" section, this chapter). Sandy silt- and silt-sized serpentines from Cores 125-779B-1R, and 125-779A-2R were deposited during or after the early Pleistocene on the basis of nannofossils found in Sections 125-779B-1R-CC and 125-779A-2R-5.

Abundant aragonite in these serpentine flows is unusual in waters this deep on the forearc (Haggerty, 1987c). Seawater below a few hundred meters in the present-day Pacific is undersaturated with respect to aragonite (Li et al., 1969; Berner and Honjo, 1981), and the aragonite compensation depth is less than 1000 mbsl in the Pacific, usually as shallow as 400 mbsl (Berger, 1970). The delicate, acicular aragonite crystals (up to 3 mm long and 0.5 mm wide) in the clay and serpentine imply authigenic growth after the serpentine was emplaced. The aragonite needles are not detrital; these needles would have been broken by flow or by transport as detrital particles.

Unit II

Sections 125-779A-3R-CC to 125-779A-35R-1, 133 cm; depth, 10.6–303.0 mbsf.
Age: early Pleistocene(?) to early Pliocene(?)/late Miocene(?).

Lithologic Unit II contains clasts of various igneous and metamorphic rock types (see "Igneous and Metamorphic Petrology" section, this chapter) in a serpentine matrix. This matrix is bluish-gray (5B 5/1) to light gray (N7) downhole to Core 125-779A-11R, with transitions to pale green (5G 6/2) and dark green (5G 3/2). The matrix is clayey silt-sized serpentine composed of 73% to 90% serpentine, 5% to 10% amphibole, 5% to 10% opaque minerals, 0% to 15% zoisite, 0% to 25% thulite, 0% to 5% chlorite, with trace amounts of garnet, epidote, plagioclase, and olivine. The unit is divided into two subunits because sedimentary strata having primary sedimentary structures are intercalated in the lower portion of the unit. The division of the subunits may be artificial because of poor core recovery and the probability that unconsolidated matrix material and sediment were washed away during the coring process.

Subunit IIA: Sections 125-779A-3R-CC to 125-779A-26R-3, 150 cm; depth, 10.6–216.2 mbsf.

The matrix of Subunit IIA is typically highly deformed by drilling, although in some cases primary structural features can be observed. In Cores 125-779A-7R, 125-779A-9R, and 125-779A-10R, the matrix appears to be sheared; in Cores 125-779A-13R, 125-779A-15R, and 125-779A-18R, the matrix has a phacoidal, sheared texture (see "Structural Studies" section, this chapter, for further description and discussion).

Subunit IIB: Sections 125-779A-27R-1, 0 cm, to 125-779A-35R-1, 133 cm; depth, 216.2–303.0 mbsf.

Smear-slide analysis of the sedimentary strata in Cores 125-779A-27R, 125-779A-28R, and 125-779A-32R of Subunit IIB revealed trace amounts of carbonate grains and kerogen(?), and up to 10% filamentous opaque mineral aggregates (tentatively interpreted as remnants of filamentous bacteria). Kerogen is usually interpreted as a detrital particle because it typically is insoluble and does not migrate through the sediment. If kerogen is present in this subunit, then it indicates a primary sedimentary origin, rather than a tectonic or igneous origin, for the subunit.

Faint horizontal bedding and sedimentary structures were also observed in the sediments of Subunit IIB, suggesting a primary sedimentary origin. Clay layers containing filamentous opaque mineral aggregates are horizontal; these separate layers display deformation structures in the serpentine matrix among the blocks of igneous and metamorphic lithologies. These clay layers may represent periods of exposure on the seafloor or hiatuses between episodes of deformation. If the filamentous opaque mineral aggregates represent bacteria that grew at or near the sediment/water interface, then these horizontal beds separate different events of serpentine deposition.

Sparse nannofossils of late Miocene/early Pliocene age were deposited with reworked Oligocene nannofossils in the strata from Core 125-779A-27R (Sample 125-779A-27R-1, 60 cm; see "Biostratigraphy" section, this chapter). The presence of the fossils also confirms the sedimentary origin of the strata in Core 1225-779A-27R. No additional microfossils were found in Unit II. The base of Unit II thus has been interpreted as having been deposited during or prior to the early Pliocene. An early Pleistocene age, determined from sediments in the core-catcher sample of Core 125-779A-2R, limits the youngest time of deposition of Unit II.

Unit III

Sections 125-779A-36R-1, 0 cm, to 125-779A-37R-CC; depth, 303.0–317.2 mbsf.

Unit III is composed of serpentine microbreccia having convolute structures. A description and discussion of the breccia clast lithologies are given in the "Igneous and Metamorphic Petrology" section (this chapter). The light greenish-gray to dark greenish-gray (5G 5/2 to 5G 8/2) matrix of the breccia is composed of serpentine (70%–90%), opaque minerals (4%–10%), chlorite (0%–20%), zoisite (0%–14%), amphibole (0%–5%), micrite (trace to 5%), and 0% to trace amounts of garnet, dolomite, and organic debris. These convolute structures strongly resemble deformation structures produced by tectonic or gravitational flow processes (for further discussion see "Structural Studies" section, this chapter). In Section 125-779A-36R-3, there is a dusky red (5R 3/3) iron oxide staining the matrix and coating pebbles, similar to that observed in the matrix at the base of Subunit IIB at Site 778.

X-Ray Diffraction Analysis

XRD analyses were performed on the less than 4-mm fraction of five selected samples from Site 779 (Table 3). Although we expected to find smectite, none was observed. The sample nearest the sediment surface contained traces of an expandable chlorite. No other expandable clays were observed.

Table 3. X-ray diffraction analyses for selected samples from Site 779.

Sample	Serpentines		Talc	Fayalite
	Chrysotile	Antigorite		
125-779A-2R-3, 39 cm	***	***		
2R-3, 88 cm	***	***	*	
2R-4, 38 cm	***	***	*	
19R-1, 40 cm	***			(*)
125-779B-1R-4, 98 cm	***	***	*	

*** = Major components; * = Minor components.

The less than 4-mm fraction of the clayey silt-sized serpentine is composed entirely of serpentine, probably at least two phases (chrysotile and antigorite). Minor amounts of talc are present in some samples.

BIOSTRATIGRAPHY

Evidence from calcareous nannofossils and planktonic foraminifers indicates that the sedimentary interval overlying the serpentine in Holes 779A and 779B ranges in age from early to middle Pleistocene. A sediment interval in Core 125-779A-27R was dated as early Miocene(?) to late Pliocene(?) on the basis of calcareous nannofossils.

Calcareous Nannofossils

Hole 779A

A moderately preserved, but rare, Pleistocene nannofossil assemblage is present in Samples 125-779A-1R-CC, 125-779A-2R-3, 70 cm, and 125-779A-2R-5, 53 cm. In Sample 125-779A-1R-CC, the nannofossil assemblage is characterized by *Gephyrocapsa oceanica*, *Ceratolithus telesmus*, *C. simplex*, and by the absence of *Emiliania huxleyi*. This assemblage is late middle Pleistocene (CN14b) in age, based on the Okada and Bukry (1980) zonation. Sample 125-779A-2R-3, 70 cm, contained *Pseudoemiliania lacunosa*, *Gephyrocapsa oceanica* and *G. caribbeanica*. Thus, the age could be defined as early to middle Pleistocene (Subzone CN14a). In Sample 125-779A-2R-5, 53 cm, the last occurrence of *Calcidiscus macintyrei*, together with *Pseudoemiliania lacunosa* and *Gephyrocapsa oceanica*, was noted. The highest occurrence of *Calcidiscus macintyrei* is at the base of CN14a; thus, the assemblage was assigned to the early Pleistocene.

Sample 125-779A-27R-1, 60 cm, contains a sparse assemblage. We assume that it is late Miocene/early Pliocene in age, based on the occurrence of *Cricolithus jonesi*, *Reticulofenestra pseudoumbilica*, and *Discoaster variabilis*. Reworked *Dictyococcites bisectus*, *Cyclicargolithus floridanus*, and *C. bisectus* (all latest Oligocene) also are present.

Hole 779B

Moderately to well-preserved, rare-to-few Pleistocene nannofossil assemblages are present in Samples 125-779B-1R-1, 89–91 cm; 125-779B-1R-6, 91–92 cm; and 125-779B-1R-CC. In Sample 125-779B-1R-1, 89–91 cm, the assemblage is characterized by *Pseudoemiliania lacunosa*, *Helicosphaera sellii*, *Gephyrocapsa oceanica*, and *Ceratolithus cristatus*; it is early Pleistocene in age (CN14a) on the basis of Okada and Bukry's (1980) zonation. Sample 125-779B-1R-6, 91–92 cm, shows a comparable association and thereby age. In Sample 125-779B-1R-CC, the last occurrence of *Calcidiscus macintyrei* was found together with the assemblage above, which dates this sample as early Pleistocene (CN14a).

Foraminifers

A sparse, poorly preserved, Quaternary planktonic foraminiferal assemblage was recovered from Sample 125-779A-1R-CC. This sample contained rare specimens of fragmented *Globorotalia (M.) menardii*.

The Pleistocene age (Zone N22) was determined by the sinistral coiling of *G. menardii*, a characteristic of post-Pliocene/Pleistocene boundary forms. Older forms exhibit dominantly dextral coiling. Sample 125-779B-1R-CC was barren.

Diatoms

Moderately preserved diatoms, mainly fragments of the extremely large diatom *Ethmodiscus rex*, were noted in Samples 125-779A-1R-1, at 5, 10, 15, and 20 cm; 125-779A-1R-CC; and 125-779B-1R-CC. Fragments of *E. rex* were common constituents of the diatom assemblage, together with rare *Nitzschia marina* and *Thalassiothrix longissima*. Sample 125-779A-2R-CC was barren of siliceous microfossils. Age-diagnostic taxa (Barron, 1985) were not observed.

IGNEOUS AND METAMORPHIC PETROLOGY

The clasts recovered in this hole comprise about 95% variably serpentinized and tectonized ultramafic and about 5% metamorphosed mafic rocks. Of the ultramafic rocks, about 80% are harzburgite and 20% are dunite. About 60% of the mafic rocks are metabasalts, and the rest are metamicrogabbros. Cores contain maximum continuous recovery of rock through intervals of up to about 150 cm long, enclosed in a sheared and deformed serpentinite matrix that is described in the "Structural Studies" section (this chapter). Contact relationships between the ultramafic and mafic rocks are ambiguous. In some of the mafic units, chilling and/or shearing and annealing along the contacts may have taken place. The intensity of serpentinization appears to decrease downhole.

Ultramafic Rocks

Serpentinized and Tectonized Harzburgites

The harzburgites are massive and vary from light to dark gray (where relatively fresh) to dark gray-green (where serpentinized). The primary mineralogy of these rocks is olivine, orthopyroxene, chromium-spinel, and subordinate clinopyroxene. The modal abundance of orthopyroxene varies from about 10% to 40%, with olivine forming most of the remainder. Clinopyroxene (1–3 modal%) is present as ubiquitous exsolution lamellae in orthopyroxene and as <1-mm blebs and anhedral crystals, typically closely related to orthopyroxene. Chromium-spinel exists in trace amounts to about 2 modal% and contains rare, brightly reflective grains that may be a sulfide mineral or a metallic alloy (rich in platinum-group elements).

The harzburgites have experienced penetrative deformation. Typically, orthopyroxene crystal morphologies range from equant to raggedly elongate; the cleavage surfaces and extinction are wavy; kink-banding is common; and fine clinopyroxene exsolution lamellae are bent. Elongate crystals (<15 mm long) and intracrystalline glide planes characterize some olivine morphologies, but microgranular and granuloblastic (1-mm equant crystals) fabrics, indicative of relatively high-temperature shear, also are present. Chromium-spinel crystals range from equant (<0.2 mm in size) to disrupted dumbbell-type shapes; locally, "trains" or "stringers" of these elongate spinels define a crude lineation parallel to elongate olivine and orthopyroxene. In the orthopyroxene-rich types, rounded olivines sometimes are included in orthopyroxene.

The degree of serpentinization is extremely variable. In some samples, most of the olivine and orthopyroxene has been replaced by mesh-textured serpentine (antigorite-rich) and relict bastite, respectively. In these strongly serpentinized types, all of the chromium-spinel (translucent in shades of deep reddish-brown/green) has been replaced by an opaque oxide mineral, probably magnetite. In some samples, this transformation process is incomplete. These partially altered spinels have original chromium-rich translucent cores, rims of magnetite, and radially arranged halos of microcrystalline chlorite (probably penninite). This type of alteration has also penetrated cracks in the original spinel grains.

Numerous veins of serpentine (up to about 40 mm wide) cut the harzburgites; many of these veins recorded a polystage history of filling. The degree of serpentinization of the harzburgite may be enhanced by the proximity to veins, and many of the breaks in the core may have taken place along veins. The largest veins generally dip at about 60° to 80°, but other conjugate and anastomosing sets with variable dip also are present. Antigorite or lizardite fills most of these veins. Some veins contain chrysotile that has grown both parallel to the original fracture walls and as discontinuous, crosscutting subsets (e.g., Section 125-779A-26R-2; Fig. 3). Subordinate brucite also is present. Shearing dislocated spinel trains in a few samples during the formation of serpentine veins. In some samples, orthopyroxene adjacent to veins has been altered to chlorite. Typically, serpentinization affected olivine the most, orthopyroxene less, and clinopyroxene the least. However, in several samples, serpentinization may have affected orthopyroxene more than olivine.

Serpentinized and Tectonized Dunites

These rocks range from deep greenish-black to black, are generally massive, and sometimes grade to harzburgite over distances of a few millimeters. Possibly, this modal change reflects original cumulus layering. The primary mineralogy consists of 90% to 99% olivine, 1% to 9% orthopyroxene, and up to 1% spinel. Most dunites have been serpentinized extensively, exhibiting mesh texture development and splays of antigorite, and are cut by numerous serpentine-rich veins. Some pieces contain crudely aligned, elongate (<15 mm), and irregularly shaped olivine that tends to form a sheared fabric. Microgranulation of olivine, intracrystalline glide planes (olivine), kink-banding (relict bastite), and elongation of spinel all provide evidence of penetrative tectonism. Deformation of exsolution lamellae of clinopyroxene in orthopyroxene is further evidence of strain in these rocks.

Although a higher proportion of primary orthopyroxene than olivine survived serpentinization, an unusually large amount of relict fresh olivine persists in a few samples, despite transformation of almost all of the orthopyroxene to serpentine. Spinel is completely altered to magnetite in the serpentinized portions. Other secondary minerals include chlorite and brucite.

Metabasalt and Metamicrogabbro

These rock types occur primarily as isolated clasts, but also form more continuous, individual core pieces reaching lengths of about 10 to 20 cm. The intact upper contact of approximately 3 m of mafic-microgabbroic material with serpentinized ultramafic rocks is present in Core 125-779A-31R. These mafic rocks range from greenish-white to dark green; in general, they are aphyric to microphyric and have an original primary mineralogy that consists of subequal proportions of plagioclase and augite. Relict subophitic texture has been preserved in one clast in Core 125-779A-9R. Originally, considerable amounts of glass were present in some of these types (30%–40%), although extensive replacement by chlorite and/or clay minerals has subsequently taken place.

Several samples are brecciated and veined by carbonate and chlorite. Prehnite is also present in "bow-tie" form (with wavy extinction as a vein-filling phase) together with pumpellyite. Pumpellyite is a constituent of the altered matrix in some samples. Sphene and albite also are scattered as metamorphic alteration products. Several zones of in-

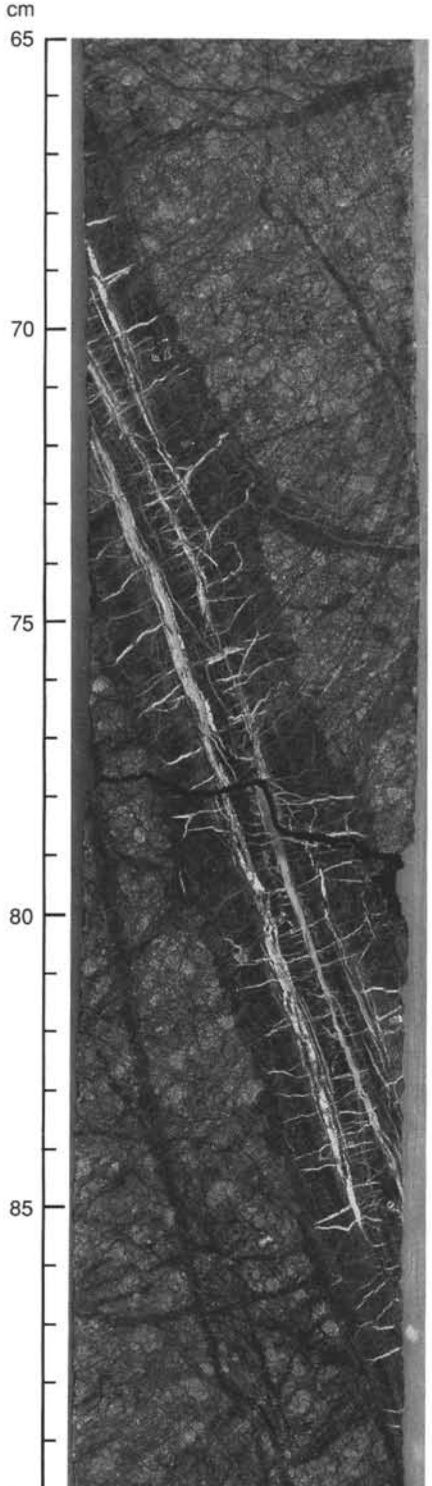

Figure 3. Interval 125-779A-26R-2, 65–90 cm, with a polyphase serpentine vein dipping at 75°, cutting tectonized, serpentinized harzburgite. The white phase is mostly chrysotile.

tense shearing traverse the mafic unit, as illustrated in the "Structural Studies" section (this chapter), and perhaps the contacts of this rock with the surrounding materials have also been sheared. A clear gradation in crystal size is present within this unit from microcrystalline at the margins to 1- to 2-mm relict subophitic in the center, and the unit may represent a sill or dike.

IGNEOUS AND METAMORPHIC GEOCHEMISTRY

Geochemical analyses of clasts entrained within the serpentinite diapir at Site 779 were performed for 32 samples of serpentinized, tectonized ultramafic rocks, for both harzburgites (21 samples) and dunites (11 samples), and for five samples of metamorphosed mafic rocks. The mafic samples range from originally glassy to moderately crystalline (diabase). The diabase comprises a 300-cm-thick zone bounded by glassy margins and is apparently of intrusive origin. Rock descriptions are presented in the "Igneous and Metamorphic Petrology" section (this chapter). Preparation and analytical techniques are given in the "Explanatory Notes" (this volume). The geochemical data are given in Tables 4 through 7.

Ultramafic Samples

Modal estimates of the original (pre-serpentinization) composition of ultramafic samples range from 10% to 25% orthopyroxene and 75% to 85% olivine in the harzburgite samples, and from 1% to 10% orthopyroxene and 90% to 99% olivine in the dunite samples. Both rock types contain 1% clinopyroxene and spinel. All samples are variably serpentinized (25%–100%) and frequently tectonized. All ultramafic samples are remarkably homogeneous chemically (Tables 4 and 5) and standard deviations are small.

Major-Element Chemistry

Loss on ignition (LOI) of these samples ranges from 4.77 to 17.41 and exhibits positive correlation with percentage of serpentinization (Fig. 4). These values also correlate with bulk rock density. (See "Physical Properties" section, this chapter, for details; see "Igneous and Metamorphic Geochemistry" section, Site 778 chapter, and "Explanatory Notes," this volume, for an explanation of LOI.) Although ranges of concentrations of major elements are similar in dunite and harzburgite samples (Table 4), some small distinctions exist. SiO_2 ranges from 29.39 to 40.80 wt% in both harzburgite and dunite samples, and MgO is slightly higher in the dunite samples (38.94 to 43.43 wt%) than in the harzburgite samples (37.34 to 42.69 wt%). Al_2O_3 is slightly lower in the dunites (0.07 to 0.60 wt%) than the harzburgites (0.21 to 0.88 wt%); Fe_2O_3 is also lower in the dunites (5.66 to 8.05 wt%) than in the harzburgites (7.00 to 9.04 wt%). Magnesium number (Mg# = Mg/(Mg + Fe) × 100) is high in all rocks, ranging from 89.84 to 93.65. Na_2O and P_2O_5 are uniformly 0.0 wt%, and K_2O ranges from 0 to 0.3 wt% with one exception: Sample 125-779A-24-1, 36–38 cm, a dunite that contains 4.00 wt% K_2O and high strontium contents. In all rocks, SiO_2 and MgO are inversely correlated with LOI and percentage of serpentinization (Figs. 4A, 4B, and 4C; Table 4). The correlations with LOI are not necessarily significant, however, because of the effect of autocorrelation, whereby the sum of oxides is constrained to about 100%.

Trace-Element Data

Trace-element data are presented in Table 5. Compatible elements are predictably high in both the dunite and harzburgite samples: chromium ranges from 1216 to 2917 ppm, and nickel from 2171 to 2541 ppm, with the exception of a single

Table 4. Tabulated major-element data for serpentinized, ultramafic rocks from Site 779.

	Dunites												Harzburgites			
Hole:	779A	779A	779A	779A	779A	779A	779A	779A	779A	779A	779A		779A	779A	779A	779A
Core:	3R-CC	8R-1	10R-1	14R-1	14R-2	15R-2	16R-1	19R-2	22R-2	24R-1	25R-1	Dunite	4R-1	5R-2	5R-2	6R-1
Interval (cm):	13–15	90–93	40–43	74–77	21–24	24–27	19–23	97–99	18–20	36–38	85–87	Average	27–30	34–37	40–43	18–20
SiO_2	36.74	39.47	38.14	38.30	35.25	35.54	40.80	39.21	39.47	34.50	34.44	37.30	33.64	36.46	35.12	37.57
TiO_2	0.00	0.00	0.00	0.00	0.00	0.00	0.00	0.00	0.00	0.00	0.00	0.00	0.00	0.00	0.00	0.00
Al_2O_3	0.39	0.28	0.63	0.38	0.07	0.07	0.60	0.19	0.4	0.46	0.12	0.30	0.20	0.21	0.21	0.77
Fe_2O_3	7.38	7.63	8.08	7.33	7.14	5.66	8.05	8.15	7.36	7.31	7.02	7.40	7.04	7.71	7.23	7.72
MnO	0.10	0.11	0.12	0.10	0.09	0.08	0.10	0.12	0.10	0.11	0.09	0.10	0.14	0.09	0.10	0.11
MgO	40.31	41.21	41.19	41.71	41.35	42.14	43.43	44.36	40.95	38.94	43.40	41.70	40.13	40.18	39.87	39.61
CaO	0.14	0.15	0.60	0.44	0.10	0.21	0.54	0.25	0.15	0.37	0.20	0.30	0.07	0.22	0.08	0.55
Na_2O	0.00	0.00	0.00	0.00	0.00	0.00	0.00	0.00	0.00	0.00	0.00	0.00	0.00	0.00	0.00	0.00
K_2O	0.02	0.00	0.00	0.01	0.00	0.02	0.01	0.00	0.00	4.00	0.00	0.40	0.00	0.02	0.00	0.01
P_2O_5	0.00	0.00	0.00	0.00	0.00	0.00	0.00	0.00	0.00	0.00	0.00	0.00	0.00	0.00	0.00	0.00
NiO	0.28	0.28	0.30	0.31	0.30	0.45	0.32	0.32	0.27	0.29	0.34	0.32	0.31	0.29	0.28	0.28
Cr_2O_3	0.42	0.39	0.41	0.35	0.21	0.19	0.33	0.22	0.30	0.25	0.32	0.31	0.24	0.19	0.24	0.26
LOI	14.18	9.55	9.28	9.00	14.64	16.71	4.77	6.22	9.26	16.27	12.77	11.20	16.66	14.62	16.35	12.42
Total	99.27	98.39	98.06	97.27	98.64	98.42	98.31	98.50	97.74	101.97	98.05	98.60	98.54	98.83	98.95	98.75
Mg#	91.54	91.45	90.99	91.85	91.98	93.65	91.45	91.51	91.68	91.35	92.45	91.78	91.16	91.88	91.62	91.04
% SERP	80	78	55	70	85	85	17	35	85	93	85	69.8	100	40	93	78

Data (in wt% oxides) are from whole-rock analyses by XRF. LOI is loss on ignition between 150° and 1030°C; % SERP = percentage of serpentinization estimated from thin sections.

Table 5. Tabulated trace-element data for serpentinized, ultramafic rocks from Site 779.

	Dunites												Harzburgites			
Hole:	779A	779A	779A	779A	779A	779A	779A	779A	779A	779A	779A		779A	779A	779A	779A
Core:	3R-CC	8R-1	10R-1	14R-1	14R-2	15R-2	16R-1	19R-2	22R-2	24R-1	25R-1	Dunite	4R-1	5R-2	5R-2	6R-1
Interval (cm):	13–15	90–93	40–43	74–77	21–24	24–27	19–23	97–99	18–20	36–38	85–87	average	27–30	34–37	40–43	18–20
Nb	tr	tr	tr	tr	tr	tr	tr	tr	tr	tr	tr	tr	tr	tr	tr	tr
Zr	1	1	1	0	0	1	1	1	1	1	1	1	1	1	1	1
Y	nd	0	2	1	nd	nd	0	1	1	0	nd	0	nd	1	0	0
Sr	2	2	2	4	0	4	0	nd	1	21	3	4	5	14	6	8
Rb	1	0	nd	1	0	1		nd	nd	nd	0	0	0	1	nd	0
Zn	31	36	35	34	22	33	37	33	31	46	33	34	44	32	49	35
Cu	1	2	7	nd	1	nd	5	4	2	2	3	2	2	2	4	1
Ni	2238	2208	2396	2446	2398	3527	2512	2520	2163	2667	2486	2424	2290	2203	2171	2302
Cr	2903	2650	2796	2396	1144	1319	2236	1509	2024	1688	2167	2103	1667	1278	1629	1752
V	25	22	42	22	12	11	32	13	29	23	8	22	15	21	19	29
Ce	tr	tr	tr	tr	tr	tr	tr	tr	tr	tr	tr	tr	tr	nd	nd	nd
Ba	tr	13	tr	tr	tr	nd	13	nd	12	tr	nd	tr	tr	20	tr	21

Data (in ppm) are from whole-rock analyses by XRF; nd = not detected (background count was greater than sample count); tr = below the detection limit (<5 ppm for Nb; <10 ppm for Ba and Ce).

dunite (Sample 125-779A-15R-2, 24–27 cm) that contains 3527 ppm nickel and a single harzburgite (Sample 125-779A-22R-1, 58–60 cm) that contains 3914 ppm chromium. Chromium and nickel do not correlate with one another or with the degree of serpentinization. Niobium, zirconium, yttrium, rubidium, and titanium are all present at trace levels or are below detection limits. Values of cesium and barium are typically below detection limits, although four samples have barium values of 16 ppm or greater. Strontium, zirconium, and vanadium are slightly lower in the dunites (Sr = 4 ppm; Zn = 34 ppm; V = 8–42 ppm) than in the harzburgites (Sr = 8 ppm; Zn = 39 ppm; V = 4–50 ppm). A single dunite sample (125-779A-24R-1, 36–38 cm) has a strontium value of 21 ppm. No significant correlation exists between geochemical parameters and depth below the seafloor.

The samples analyzed from Site 779 are similar to those from Site 778 (see "Igneous and Metamorphic Geochemistry" section, Site 778 chapter, this volume), although the concentrations of several elements may be slightly different between

Table 6. Tabulated major-element data for mafic rocks from Site 779.

	Group 1 779A 9R-1 106–108	Group 2 779A 31R-1 119–121	779A 31R-2 103–105	779A 31R-3 32–34	779A 31R-CC 39–41 (cm)
SiO_2	43.45	39.47	38.32	36.88	38.45
TiO_2	2.50	1.41	1.40	1.26	1.48
Al_2O_3	14.92	12.07	14.59	12.19	13.81
Fe_2O_3	12.06	11.04	11.96	10.34	11.66
MnO	0.15	0.21	0.18	0.17	0.18
MgO	7.63	11.43	7.49	6.3	17.57
CaO	7.34	18.24	21.71	21.54	21.09
Na_2O	4.07	0.00	0.00	0.00	0.00
K_2O	0.52	0.00	0.00	0.00	0.00
P_2O_5	0.22	0.09	0.08	0.08	0.09
LOI	5.44	4.47	4.02	9.76	3.96
TOTAL	98.30	98.42	99.74	98.53	98.30
Mg#	53.01	64.85	52.77	52.10	53.66

Data (in wt% oxides) are from whole-rock analyses by XRF. LOI is loss on ignition between 150° and 1030°C.

Table 7. Tabulated trace-element data for mafic rocks from Site 779.

	Group 1 779A 9R-1 106–108	Group 2 779A 31R-1 119–121	779A 31R-2 103–105	779A 31R-3 32–34	779A 31R-CC 39–41 (cm)
Nb	tr	tr	tr	tr	tr
Zr	187	85	82	81	85
Y	48	35	34	34	35
Sr	169	92	49	62	58
Rb	10	nd	nd	nd	nd
Zn	132	94	104	93	99
Cu	51	49	38	56	55
Ni	52	57	72	69	75
Cr	163	130	196	207	219
V	424	345	339	334	337
Ce	23	tr	nd	tr	15
Ba	27	59	32	33	50

Data (in ppm) are from whole-rock analyses by XRF; nd = not detected (background count was greater than sample count); tr = below detection limits (<5 ppm for Nb; <10 ppm for Ba and Ce).

Table 4 (continued).

									Harzburgites								
779A 8R-1 45–48	779A 8R-1 57–60	779A 9R-2 52–54	779A 11R-1 .14–18	779A 12R-1 38–42	779A 13R-1 2–5	779A 13R-2 52–54	779A 14R-2 139–141	779A 16R-2 74–77 (cm)	779A 17R-2 14–17	779A 17R-3 77–80	779A 22R-1 58–60	779A 22R-1 63–65	779A 22R-3 55–57	779A 26R-3 50–52	779A 26R-2 101–103	779A 28R-3 26–28	Harzburgite average
38.35	29.39	35.45	36.49	36.81	32.18	38.62	38.08	38.70	40.20	37.37	29.13	38.61	38.09	39.61	37.09	35.53	36.26
0.00	0.00	0.00	0.00	0.00	0.00	0.00	0.00	0.00	0.00	0.00	0.00	0.00	0.00	0.00	0.00	0.00	0.00
0.49	0.57	0.28	0.41	0.19	0.25	0.66	0.88	0.64	0.37	0.30	0.29	0.17	0.10	0.69	0.63	0.19	0.40
7.69	9.04	7.47	7.00	7.50	8.15	7.77	7.35	7.38	7.36	6.98	9.25	7.47	7.76	8.11	7.08	7.07	7.63
0.11	0.17	0.10	0.10	0.10	0.12	0.11	0.11	0.11	0.10	0.09	0.17	0.11	0.11	0.11	0.10	0.10	0.11
40.00	41.22	41.32	39.14	41.50	40.35	40.03	37.34	39.33	42.69	39.47	41.26	41.84	42.96	40.95	39.50	39.32	40.38
0.53	0.14	0.36	0.50	0.33	0.32	0.79	0.81	0.62	0.35	0.29	0.16	0.23	0.13	0.80	0.58	0.35	0.39
0.00	0.00	0.00	0.00	0.00	0.00	0.00	0.00	0.00	0.00	0.00	0.00	0.00	0.00	0.00	0.00	0.00	0.00
0.01	0.00	0.01	0.01	0.01	0.00	0.00	0.02	0.03	0.01	0.01	0.00	0.01	0.00	0.00	0.00	0.00	0.01
0.00	0.00	0.00	0.00	0.00	0.00	0.00	0.00	0.00	0.00	0.00	0.00	0.00	0.00	0.00	0.00	0.00	0.00
0.29	0.32	0.31	0.28	0.29	0.30	0.29	0.28	0.28	0.32	0.30	0.33	0.30	0.30	0.29	0.28	0.29	0.30
0.37	0.41	0.22	0.24	0.21	0.33	0.27	0.43	0.32	0.28	0.26	0.57	0.42	0.18	0.29	0.24	0.25	0.30
11.01	17.41	14.03	14.83	12.33	16.87	11.28	13.82	11.46	6.81	15.40	16.93	10.01	9.17	8.57	13.32	15.63	13.28
98.19	97.95	99.02	98.48	98.76	98.24	99.27	98.42	98.27	97.90	98.92	97.19	98.44	98.32	98.84	98.30	98.19	98.47
91.16	90.03	91.64	91.72	91.64	90.75	91.08	90.96	91.35	92.00	91.81	89.84	91.73	91.65	90.91	91.70	91.68	91.29
100	100	40	98	78	100	75	50	75	25	35	75	50	60	45	35	100	69.14

Data (in wt% oxides) are from whole-rock analyses by XRF. LOI is loss on ignition between 150° and 1030°C; % SERP = percentage of serpentinization estimated from thin sections.

Table 5 (continued).

									Harzburgites								
779A 8R-1 45–48	779A 8R-1 57–60	779A 9R-2 52–54	779A 11R-1 14–18	779A 12R-1 38–42	779A 13R-1 2–5	779A 13R-2 52–54	779A 14R-2 139–141	779A 16R-2 74–77	779A 17R-2 14–17	779A 17R-3 77–80	779A 22R-1 58–60	779A 22R-1 63–65	779A 22R-3 55–57	779A 26R-2 50–52	779A 26R-3 101–103	779A 28R-3 26–28	Harzburgite average
tr	tr	tr	tr	tr	tr	tr	tr	tr	tr	tr	tr	tr	tr	tr	tr	tr	tr
1	0	1	1	1	nd	nd	0	0	0	1	1	1	1	1	1	1	1
1	0	0	nd	nd	0	1	0	0	1	nd	0	0	0	1	nd	0	0
11	8	8	20	11	12	1	4	1	1	1	6	1	4	1	21	28	8
0	0	nd	nd	1	0	0	1	1	1	1	nd	0	1	nd	nnd	nd	0
38	63	36	36	31	56	30	39	31	30	32	57	37	32	35	36	37	39
3	3	1	1	2	1	6	10	3	4	3	2	3	3	7	2	1	3
2302	2541	2476	2181	2313	2391	2267	2185	2244	2502	2389	2571	2360	2382	2308	2185	2251	2330
2542	2841	1517	1632	1434	2256	1824	2917	2166	1920	1786	3914	2888	1216	1956	1616	1682	2021
29	41	15	24	20	16	31	50	31	32	21	23	28	8	30	24	4	24
nd	tr	tr	nd	tr	tr	15	tr	tr	tr	tr	tr	nd	tr	nd	tr	nd	tr
tr	nd	nd	tr	14	tr	tr	20	tr	tr	13	nd	tr	tr	tr	tr	17	tr

Data (in ppm) are from whole-rock analyses by XRF; nd = not detected (background count was greater than sample count); tr = below the detection limit (<5 ppm for Nb; <10 ppm for Ba and Ce).

the two sites. Values for Al_2O_3 and nickel are slightly less and slightly greater for MgO and CaO in Site 778 samples than in Site 779 samples.

Mafic Samples

Mafic samples fall into two broad categories: metabasalt (Group 1) and metadiabase (or metagabbro, Group 2). Group 1 consists of a single sample that originally contained 40 to 75 modal% glass, 10 to 15 modal% plagioclase, and 10 to 30 modal% clinopyroxene. The original assemblage has now been highly altered to clays and chlorite. The diabase samples (Group 2) are highly altered to prehnite/pumpellyite facies, but may have originally contained 60 to 70 modal% plagioclase and 20 to 40 modal% clinopyroxene.

Major-Element Analysis

One sample (125-779-9R-1, 106–108 cm) was analyzed from the metabasalt clasts (Table 6). SiO_2 (43.45 wt%), MgO (7.63 wt%), Al_2O_3 (14.92 wt%), and most other major oxides are within the normal abundance ranges for mid-ocean ridge basalts (MORBs), although the TiO_2 (2.5 wt%) is moderately high.

Samples in the metadiabase zone (125-779-31R-1, 119–121 cm, to 125-779-31R-CC, 39–41 cm) have mid-range TiO_2 (1.26–1.81 wt%), variable MgO (6.31–11.43 wt%), and low SiO_2 (36.88–39.47 wt%) values (Table 6). Abundances of Al_2O_3 range from 12.19 to 14.59 wt%, and Fe_2O_3 ranges from 10.34 to 11.96 wt%. Values for CaO are high (18.24–21.71 wt%), and neither Na_2O nor K_2O is present. This unusual chemistry may be the result of calcium replacing silicon, potassium, and sodium during prehnite/pumpellyite alteration of the samples.

Trace-Element Analysis

The single Group 1 metabasalt clast has higher incompatible elements (Zr = 187 ppm, Y = 48 ppm, Sr = 169 ppm) and vanadium (424 ppm) than the Group 2 samples, but similar compatible elements (Table 7). Abundances of compatible elements for both groups are similar and restricted in range: nickel ranges from 52 to 75 ppm and chromium from 130 to 218 ppm. The intrusive samples (Group 2) have very uniform, mid-range values for the incompatible elements of zirconium (81–85 ppm), yttrium (34–35 ppm), and strontium (50–92 ppm). Concentrations of vanadium (334–345 ppm) also are uniform, and those of rubidium below detection limits in all samples. This uniformity suggests that this zone of diabase was emplaced as a single flow or intrusion.

The differences in ratios of incompatible elements of these two groups (Fig. 5A) suggest a different source for the Group 1 clast than for the Group 2 samples. The similarity of the major-element chemistry (Table 6) and some of the trace-element chemistry (Table 7 and Fig. 5B) suggests that both groups represent MORB-type sources. The metabasalt clast from Group 1 most resembles the Group 2 clast from Site 778 in its immobile trace-element characteristics, although its Fe_2O_3 content is lower. The Group 2 metadiabase samples resemble the Group 3 clasts from Site 778, classifying as MORBs on the two discriminant diagrams used (Figs. 5A and 5B).

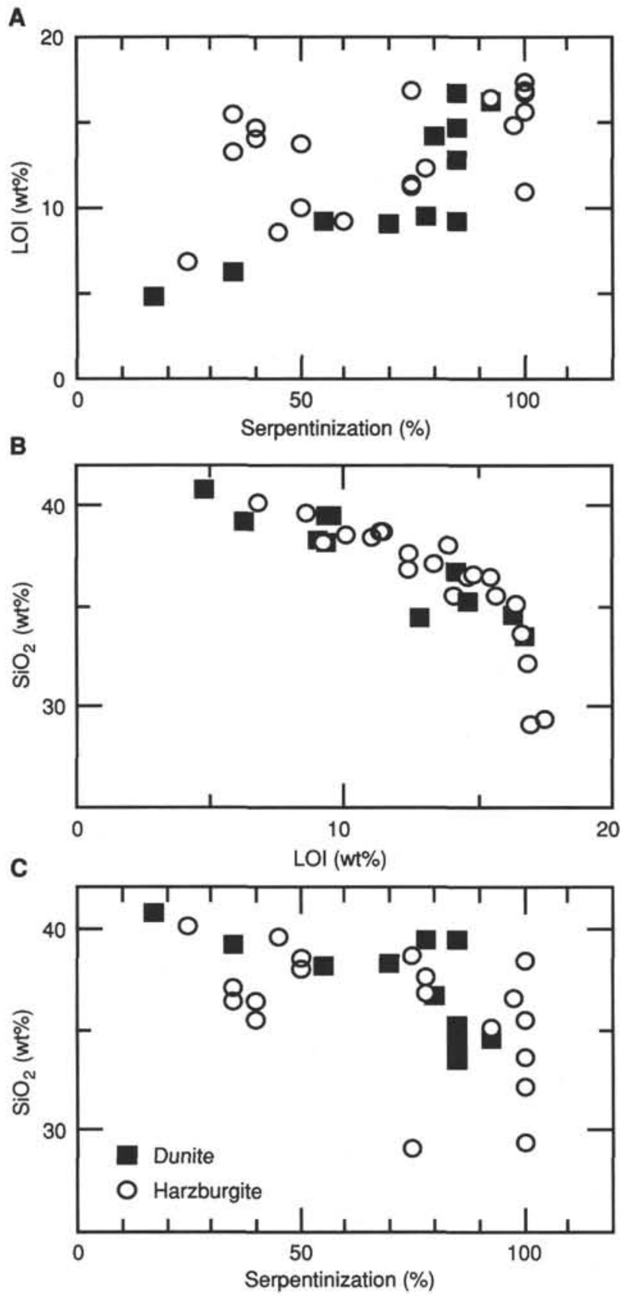

Figure 4. A. Serpentinization (modal%) vs. weight percent loss on ignition (LOI) between 105° and 1030°. B. LOI (modal%) vs. SiO_2 (wt%). C. Serpentinization (modal %) vs. SiO_2 (wt%). Filled squares represent data from dunite and open circles represent data from harzburgite.

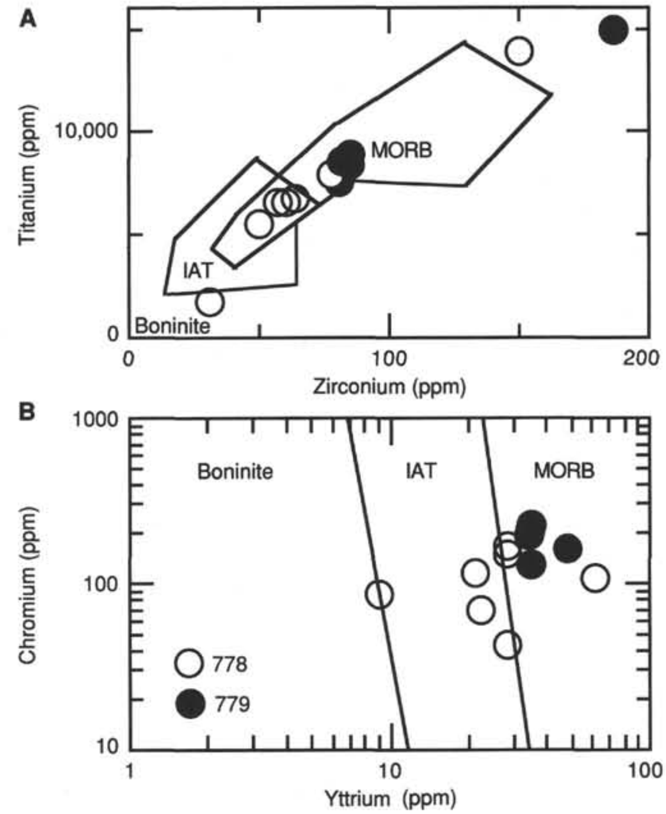

Figure 5. A. Discriminant diagram of tectonic environment for basaltic rocks using zirconium and titanium for mafic basaltic rocks. Data plotted are from mafic samples from Sites 779 and 778. Fields are from Pearce and Cann (1973). B. Discriminant diagram for tectonic environment of mafic rocks using log chromium vs. log yttrium. Data plotted are from mafic samples from Sites 779 and 778. Fields are from Pearce and Wanming (1988). Open circles represent analyses from Site 778; filled circles represent analyses from Site 779. MORB = mid-ocean ridge basalt; IT = island-arc tholeiite.

SEDIMENT/FLUID GEOCHEMISTRY

Sediment Geochemistry

Cores from Site 779 were analyzed on board ship for inorganic carbon and for total carbon, nitrogen, and sulfur using the techniques described in the "Explanatory Notes" (this volume). The organic carbon content was then calculated by difference. These results are presented in Table 8 and in Figures 6 and 7. As at Site 778, the cores are uniformly carbonate-poor, except for an interval within the upper 10 m that contains about 15 wt% $CaCO_3$. This interval was less than 6 m thick at Site 778 and at least 8 m thick at Site 779. As at Site 778, the carbonate-rich interval does not extend to the seafloor: samples from about the upper 1 m at both sites have a lower carbonate content. The concentration of organic carbon at Site 779 ranges from 0 to 0.45 wt% and may be slightly higher than that at Site 778. Although sulfur at Site 779 was not detected in most samples, the sulfur content, where detected, is 0.11 wt% and less. Therefore, the sulfur content may be lower than at Site 778. Nitrogen contents are low at both sites, ranging up to 0.15 wt% at Site 779, but are generally lower than 0.1 wt%.

Fluid Geochemistry

In marked contrast with Site 778, very high concentrations of methane and ethane were measured in the cores at Site 779 (Fig. 8). Propane was also detected in three headspace-gas samples (Table 9) and in three gas pockets sampled directly through the core liner (Table 10). One of the latter samples (from 237 mbsf) contained more than 30 vol.% methane, as well as ethane and propane. A headspace-gas sample from 227 mbsf contained 370 mL of methane per liter of wet unconsolidated serpentine. At the measured porosity of 44% in the cores at this depth, this is equivalent to 38 mM methane in the pore waters, making methane a major dissolved species.

Table 8. Total carbon, organic carbon, and carbonate carbon in cores at Site 779.

Core, section interval (cm)	Depth (mbsf)	Total carbon (%)	Inorganic carbon (%)	Organic carbon (%)	$CaCO_3$ (%)
125-779A-1R-1, 22–23	0.22		0.41		3.4
779A-1R-1, 28–29	0.28		1.17		9.8
779A-1R-1, 55–56	0.55		1.11		9.3
779A-1R-1, 76–77	0.76	2.04	2.07	0.00	17.2
779A-2R-1, 67–68	1.77		0.12		1.0
779A-2R-1, 73–74	1.83		0.14		1.2
779A-2R-1, 94–95	2.04		2.80		23.3
779A-2R-1, 134–135	2.44	2.51	2.06	0.45	17.2
779A-2R-2, 85–86	3.45		1.91		15.9
779A-2R-3, 136–137	5.46		2.01		16.7
779A-2R-4, 86–87	6.46	2.19	2.06	0.13	17.2
779A-2R-5, 36–37	7.46		1.85		15.4
779A-4R-1, 58–59	20.68	0.43	0.13	0.30	1.1
779A-5R-3, 34–35	32.89	0.29	0.12	0.17	1.0
779A-7R-1, 46–47	48.96	0.41	0.05	0.36	0.4
779A-9R-1, 32–35	68.42	0.34	0.03	0.31	0.2
779A-13R-1, 91–92	107.51	0.33	0.06	0.27	0.5
779A-18R-1, 64–67	155.54		0.05		0.4
779A-18R-2, 27–31	156.67	0.31	0.07	0.24	0.6
779A-18R-3, 4–7	157.94		0.07		0.6
779A-27R-1, 57–59	216.77	0.31	0.03	0.28	0.2
779A-28R-2, 58–59	227.05	0.25	0.05	0.20	0.4
779A-28R-2, 87–89	227.34		0.06		0.5
779A-29R-2, 33–35	236.23	0.25	0.07	0.18	0.6
779A-30R-1, 48–49	245.48	0.24	0.05	0.19	0.4
779A-32R-1, 123–125	265.63	0.26	0.04	0.22	0.3
779A-32R-2, 17–19	266.07		0.04		0.3
779A-34R-1, 95–98	284.65		0.05		0.4
779A-36R-1, 46–47	303.46	0.20	0.06	0.14	0.5
779A-36R-1, 106–108	304.06		0.25		2.1
779A-36R-2, 70–71	305.20		0.10		0.8
779A-36R-CC, 9–13	306.38		0.36		3.0
779A-37R-1, 49–50	313.19	0.17	0.03	0.14	0.2
779A-37R-2, 4–5	314.24		0.02		0.2
779A-37R-CC, 4–7	314.42		0.04		0.3
125-779B-1R-1, 0–1	0.00		0.03		0.3
779B-1R-1, 19–21	0.19		0.88		7.3
779B-1R-1, 60–61	0.60		1.54		12.8
779B-1R-1, 96–100	0.98		3.78		31.5
779B-1R-2, 9–10	1.59		1.83		15.2
779B-1R-2, 43–45	1.93		1.44		12.0
779B-1R-2, 108–109	2.58		1.52		12.7
779B-1R-3, 66–68	3.66		1.76		14.7
779B-1R-4, 48–50	4.98		1.85		15.4
779B-1R-5, 91–93	6.91		2.10		17.5
779B-1R-6, 48–50	7.98		1.23		10.2

Except for the upper 10 m, where concentrations are low, and an unsampled interval between 9 and 43 mbsf, methane and ethane concentrations were found to be high throughout the unconsolidated serpentine section. Two large spikes can be seen at 227 and 266 mbsf that are defined by only one or two samples each, but which correspond to the high concentrations of methane, ethane, and propane measured in gas pockets at 237, 275, and 285 mbsf (Table 10). These spikes correspond to maxima in the methane-to-ethane ratio as well (Fig. 8).

Interstitial waters at Site 779 (Table 11) are different from those at Site 778. Moreover, the surficial samples from Hole 779B are different from those from Hole 779A, indicating that there is considerable lateral variation in the composition of interstitial water on Conical Seamount. Results from Sites 778 and 779 are compared in Figures 9, 10, and 11. Interstitial waters from Hole 779A are much more alkaline, with pH rising from 7.5 at 4 mbsf to 11.6 at 108 mbsf (Fig. 9). From 108 to 246 mbsf, pH remains in a narrow range between 11.1 and 11.9. Below 246 mbsf it decreases again to a value of 9.9 at 314 mbsf, near the bottom of the hole. Changes in alkalinity and ammonia (Fig. 9) parallel these changes in pH. Alkalinity rises to a maximum concentration of 15 meq/kg at 246 m and then falls to 2.4 meq/kg near the bottom of the hole. Ammonia reaches a maximum of 152 mmol/kg at 246 mbsf before dropping to less than one-half that value near the bottom of the hole. The concentration of dissolved silica remains below 50 mmol/kg throughout the hole, except for samples from the upper 10 m and the lowermost two samples from 306 and 314 mbsf, which define an abrupt increase to 361 mmol/kg near the bottom of the hole. These silica-rich samples have a lower pH and are relatively poor in alkalinity and ammonia.

The usual mechanism for generating alkalinity and ammonia in the pore waters of deep-sea sediments is reduction of seawater sulfate by bacteria that oxidize buried organic matter. Sulfate does decrease by nearly a third at Site 779, but only to a depth of 108 mbsf (Fig. 9). Below that it increases again to 90% of the seawater value, before decreasing to a second minimum at 285 mbsf. No odor of H_2S was detected in any of the interstitial-water samples from Site 779. However, one would not expect a strong odor at the high pH of these samples, at which H_2S would be dissociated into nearly equal amounts of bisulfide and sulfide ions. (The second ionization constant of H_2S at 25°C is 11.96.) The probable presence of H_2S was detected by formation of a pale yellow to rusty orange to dark brown precipitate in some of the interstitial-water samples when $HgCl_2$ was added. These samples were from 108, 157, 306, and 314 mbsf in Hole 779A. This precipitate did not form in samples from 33 mbsf in Hole 779A or from 1 to 9 mbsf in Holes 779B and 778A. No other samples were tested. As noted above, the organic carbon content of these cores is low. It is highly probable from all these lines of evidence that some sulfate from the interstitial waters has been reduced to sulfide. Whether this reduction was caused by bacterial action or by inorganic processes or by both is not known.

As at Site 778, the concentration of magnesium in the interstitial waters decreases to very low values over the depth interval 0 to 100 mbsf (Fig. 10). The lowermost two samples from Hole 779A show a slight rebound, which may be real or may be an artifact of contamination with seawater during drilling and sample recovery. These are the same two samples that exhibit the large increase in silica noted above; this increase in silica is too large to have been caused by seawater contamination, even by silica-rich ocean bottom water, which contains about 150 mmol/kg silica in this area. Even if the increase in magnesium is entirely the result of seawater contamination, the other dissolved species should have been affected only negligibly, because the small size of the increase limits the amount of seawater contaminant to less than 8% to 12% of the samples.

Calcium also decreases by more than 90% at Site 779, in contrast to Site 778, where it more than doubled (Fig. 10). The decrease in calcium presumably resulted from precipitation of $CaCO_3$ in response to the large increase in alkalinity, an increase that was absent at Site 778. Potassium (Fig. 10) decreases by one-third with depth at both sites. Most of this decrease occurs within 50 m of the bottom of Holes 778A and 779A. Decreases in potassium in the interstitial waters of marine sediments commonly result from alteration of volcanic material at low temperature. The sharp decreases near the bottom of Holes 778A and 779A may indicate that volcanic material is present at these levels in these holes, and possibly also is beneath the serpentinite some distance below the maximum depths drilled. Sodium (Fig. 10) increases with depth at both Site 779 and Site 778, but the size of the increase is much greater at Site 779. Sodium reaches a maximum concentration between 108 and 227 mbsf that is 24% higher

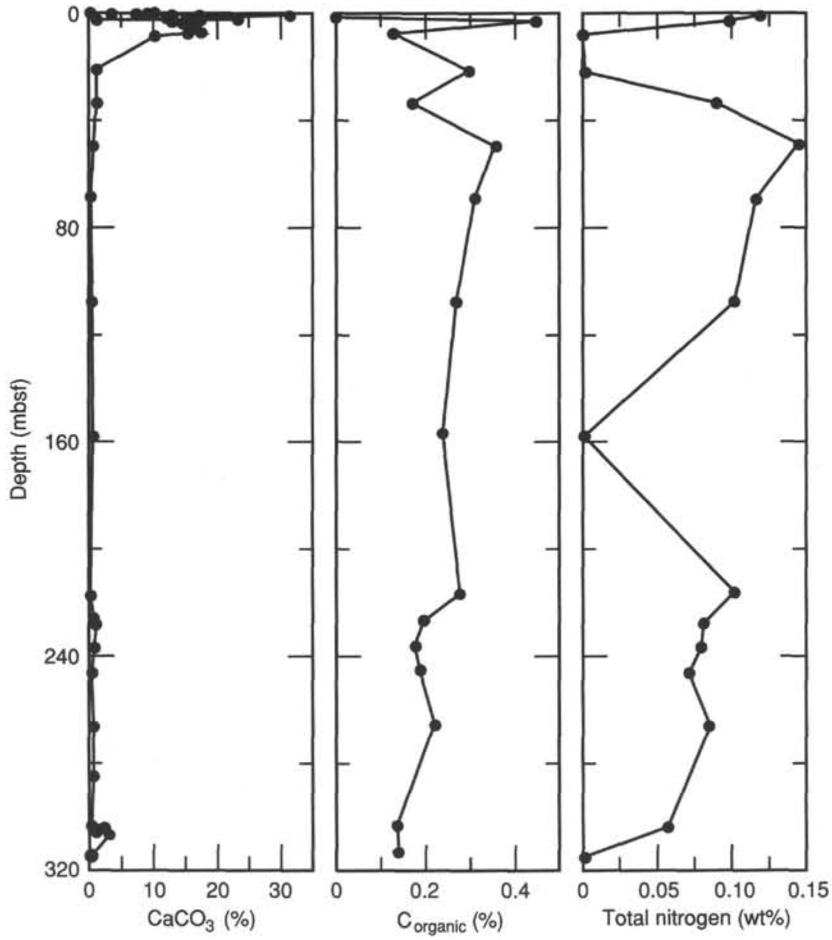

Figure 6. Calcium carbonate, total organic carbon, and total nitrogen (wt%) in cores from Holes 779A and 779B.

than that in seawater, before declining again to a minimum concentration between 274 and 306 mbsf that is still 8% higher than that in seawater. The minimum is defined by the increased sodium in the lowermost two samples, the same two that are also relatively rich in silica, sulfate, and magnesium, and poor in alkalinity, ammonia, potassium, and hydrogen ions.

The depth profiles for salinity, chlorinity, and bromide have somewhat similar shapes to that for sodium, except that salinity and chlorinity exhibit large decreases, rather than increases, relative to their seawater values (Fig. 11). As at Site 778, salinity and chlorinity decrease by about 10% with depth. As is the case for the other dissolved species, the lowermost two samples in Hole 779A reverse the prevailing trend: both salinity and chlorinity increase near the bottom of the hole.

The complexity of the pore-water profiles at Site 779, especially those for sulfate, sodium, salinity, and chlorinity, suggests the possibility of mixing between fluids, with two or more distinct compositions. One of these fluids has a distinctly lower salinity and chlorinity than seawater. Possible origins for this fluid are discussed in the "Sediment/Fluid Geochemistry" section, Site 780 chapter (this volume).

STRUCTURAL STUDIES

At Site 779, structures related to tectonic processes were found in both hard rocks (serpentinized peridotites, metagabbros, and metabasalts) and soft sediments.

Deformation Patterns in Unconsolidated Serpentine and Serpentine Sediments

In the soft sediments recovered between the serpentinized peridotite blocks in lithologic Unit II, plastic folds locally define a nonpenetrative deformation (Fig. 12), and a pervasive, repeated cleavage also is locally present. Anastomosing cleavage planes developing around soft or hard serpentinitic elements define small lenses (phacoids, Fig. 13). A spectacular shear fabric within the soft laminated serpentines exists in Interval 125-779-20R-1, 40 to 60 cm. In this interval, the general foliation is oblique to the core axis (dip angle of 50° to 60°) and is helicoidal. (This foliation is pervasive and thus does not seem to result from drilling disturbance.) An asymmetric sheared fabric is emphasized by both the external shape of the serpentinite blocks and the cleavage developed around them (Fig. 14). In Sections 125-779A-18R-1 and 125-779A-18R-2, the foliation is almost vertical. Vertical, millimeter-scale chrysotile fibers, developed within a vein 3 cm long that opened in the serpentine, define the stretching direction. The vein is deformed along the edge of the core, probably as a result of drilling disturbance (Fig. 15). Abundant, white, discontinuous, distorted laminae found within the serpentine sediments are probably remnants of similar veins that were deformed earlier. On the basis of locally intense flattening and cleavage development, the serpentinous matrix can be interpreted as a probable

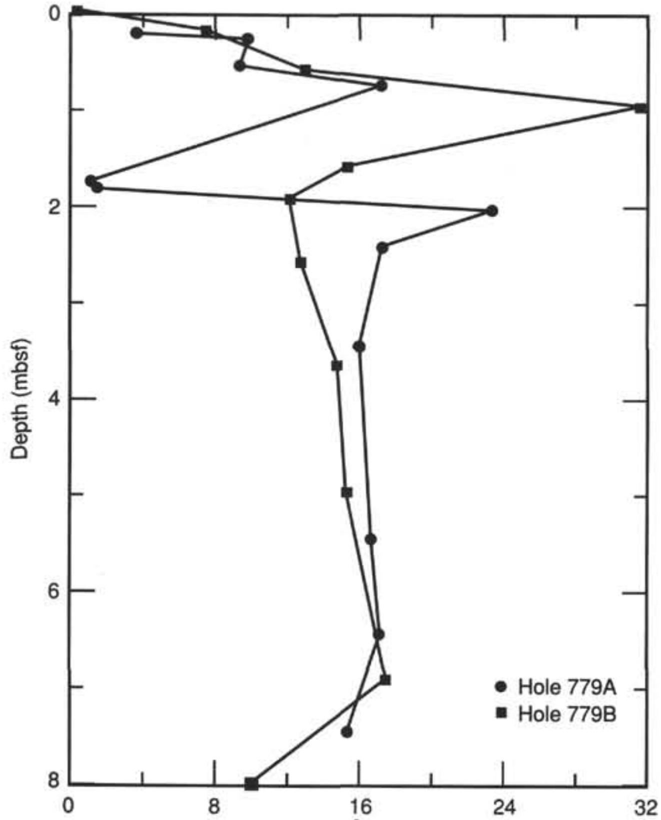

Figure 7. Calcium carbonate (wt%) in cores from Hole 779B and from the upper 8 m of Hole 779A.

fault gouge. Nevertheless, the presence of reworked subangular and unsorted serpentine debris (Interval 125-779A-30R-2, 4 to 10 cm, for example), as well as autochthonous organic matter and nannofossils in Core 125-779A-27R, demonstrate that the material is not purely tectonic in origin. It must be considered a tectonized sedimentary matrix.

Deformation patterns in lithologic Unit III of Site 779 are similar to those described in lithologic Unit II of Hole 778A. The layered serpentine microbreccias exhibit a succession of plastic folds affecting all sections of core. The term "convolute folding" thus can be used to describe the observed disturbances.

Structures and Deformation of Hard Rocks in Lithologic Unit II

Veining

The most visible structural features in the hard rocks in lithologic Subunit IIA are related to veining of the serpentinized harzburgites. Two main types of vein can be distinguished on the basis of color and habit (Fig. 16). Dark veins of antigorite corresponding to a 100% serpentinization of the peridotites have developed as a conjugate system (Fig. 16A). In some cases, the sharp edge of a vein may be observed to crosscut orthopyroxenes. This suggests that these veins do not correspond to a late filling of fractures, but to a progressive serpentinization of the initial ultramafic rocks. Locally, as shown in Figure 17, anastomosing veins define a pervasive grid that outlines elements of rhomboidal shape. These rhomboids are interpreted as the precursors of the major part of the phacoid-shaped elements in the sedimentary matrix. They may have been removed from their parent rock by alteration and softening of the completely serpentinized areas. Significantly, single or adjacent blocks within the cores have parted along the veins. Thus, many of the initial block edges most likely mark the site of early antigorite veins, rather than late shear zones. This implies that the alteration processes that softened the serpentinized peridotites may have initialized along antigorite veins.

The second type of vein consists of white, chrysotile-rich secondary fractures. These result from tensional stresses that opened the rocks. Small offsets of a few millimeters can be observed along the secondary fractures. Three subtypes, which can coexist, were observed (Fig. 16B): (1) veins located in the central part of preexisting antigorite veins parallel to the general trend of the antigorite vein; (2) veins that crosscut the subtype 1 veins and fill successive, centimeter-long tension cracks located within the dark antigorite veins ("Frankenstein" veins); and (3) veins whose distribution is unrelated to the antigorite vein structure.

The distribution of the chrysotile veins is not homogeneous along lithologic Unit II. These veins are present, but not abundant, in Cores 125-779A-3R to 125-779A-13R, are almost absent from Cores 125-779-14R to 125-779A-20R, and become abundant in Cores 125-779A-28R to 125-779A-35R.

Brecciation

Intense cataclasis leading to the development of brecciated shear lenses can be observed in some completely serpentinized samples of Sections 125-779A-30R-2 and 125-779A-31R-1 (Fig. 18). Brecciation post-dated the serpentinization and probably took place at a shallow level. Chrysotile veins crosscut the sheared fabric. Preliminary observations of hand-specimens show that the cleavage planes between the shear lenses are occupied by a light-colored mineral, probably chrysotile, suggesting that this brecciation took place in the chrysotile stability field. Detailed studies will be required to confirm this interpretation. Intense brecciation also affected some of the metagabbros and metabasalts of Core 125-779-31R.

Horizontal Schistosity

Horizontal schistosity developed locally in flattened and sheared pure serpentinites recovered in Sections 125-779A-30R-2 and 125-779A-31R-1. This pervasive schistosity is accompanied by slickensides and, in some places, by the folding of the serpentinites between two shear planes.

Foliation and Ductile-Brittle Shear Zones

Mantle foliation (high-temperature deformation) in the peridotites is not pervasive and develops only locally. It is defined by the alignment of elongated spinels and sheared orthopyroxenes (shearing along cleavages) and by microgranulation of olivines along intracrystalline glide planes. Spinel alignments may be deformed further along serpentine veins, as seen in thin section (Sample 125-779A-16R-1, 16–19 cm).

The tectonic fabrics observed in samples from Cores 125-779A-30R and 125-779A-31R are well defined. Sample 125-779A-30R-2, 34–52 cm, is a lithified tectonic breccia, representing a shear zone 20 cm thick. This zone exhibits a clear foliation defined by the alignment of elongated serpentinite clasts, some of which may have been reduced to millimeter-thick flakes. A weak stretching lineation can be observed on the top surface of the sample. The foliation is crosscut by more brittle conjugate faults. Foliation planes are bent along the fracture plane, indicating a normal sense of shear (Fig. 19). Senses deduced from analysis of other fault planes visible in this sample are consistent with a normal movement, that is, lateral extension of the sample with respect to the vertical axis of the core. The metagabbros recovered in Sections 125-779-31R-2 and 125-779-31R-3 exhibit local, mostly

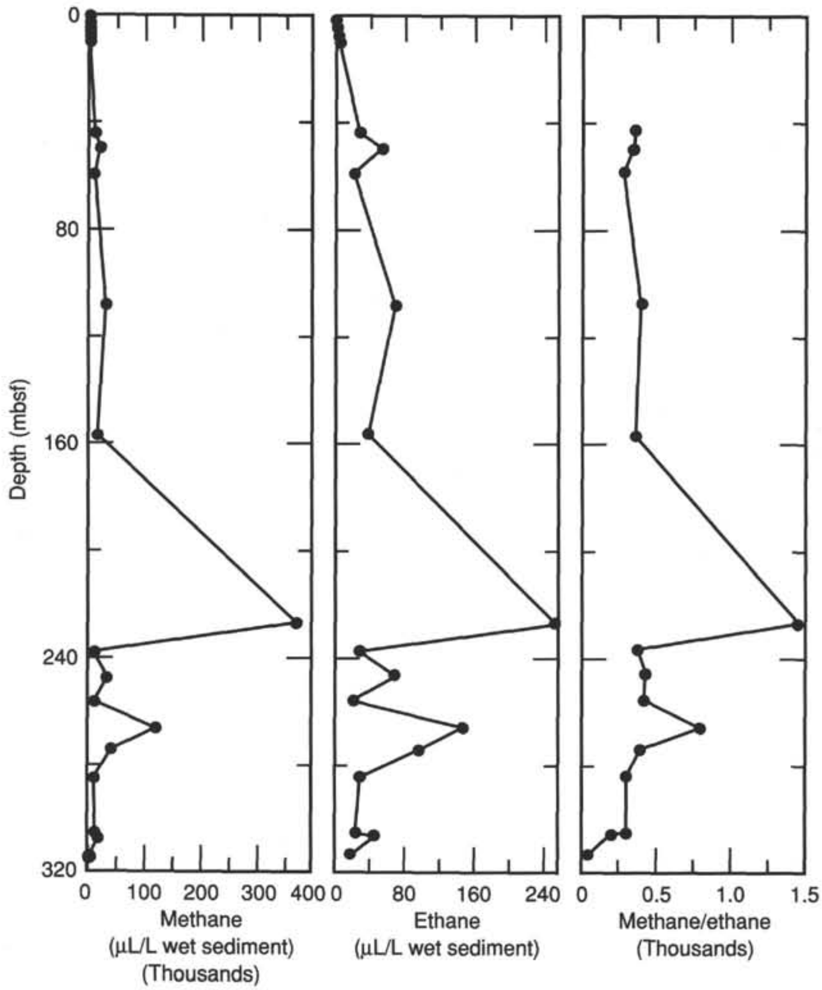

Figure 8. Methane, ethane, and the methane/ethane ratio in cores at Site 779.

horizontal, foliated zones. This early foliation represents probable deep ductile shear zones and is in turn crosscut and deformed by late, more brittle faults, similar to those described above (Fig. 20). In each case, the sense of movement determined by the bending of the foliation along the faults indicates lateral extension with respect to the core axis (Fig. 21).

Discussion

Examination of the orientation of all the veins and fractures affecting the rocks recovered at Site 779 suggests no regular arrangement between the drilled blocks. This supports the idea that lithologic Unit II represents a chaotic formation. Regarding the deformation, Subunit IIB is characterized by the development of an early foliation within the gabbroic blocks and by the presence of brittle-ductile conjugate faults, indicating lateral extension with respect to a vertical drilling axis. Deformation of the unconsolidated serpentine and serpentine sediments between the blocks may have resulted from differential movements between the blocks. This deformation may have coincided either with the rising of the diapiric material or with the lateral flow of the unconsolidated carapace covering the seamount. The presence of fossiliferous sediments within lithologic Subunit IIB, suggesting that lithologic Subunit IIA was emplaced laterally on the seafloor as a gravity nappe, favors the second hypothesis. Deformation within the sediments of lithologic Unit III is important, but might be consistent with gentle flowage under the load of lithologic Unit II.

Table 9. Results of headspace-gas analyses of cores at Site 779.

Core section, interval (cm)	Depth (mbsf)	Methane (µL/L)[a]	Ethane (µL/L)[a]	Propane (µL/L)[a]	Methane (µM)[b]
125-779A-1R-1, 97–100	1.0	4			0.3
779A-5R-3, 80–85	42.9	9,333	27		833
779A-7R-1, 70–75	49.2	18,273	54		1,631
779A-8R-1, 0–5	58.5	5,302	20		473
779A-13R-1, 135–140	108.0	28,274	69		2,523
779A-18R-1, 147–150	156.4	13,050	37		1,164
779A-28R-1, 130–135	227.1	370,202	255	23	33,033
779A-29R-1, 145–150	237.0	10,202	28	9	910
779A-30R-1, 110–115	246.1	30,128	70		2,688
779A-31R-1, 145–150	256.2	8,508	20		759
779A-32R-2, 10–15	266.0	118,320	149	11	10,558
779A-33R-1, 37–42	274.4	36,906	95		3,293
779A-34R-1, 101–105	284.7	8,236	27		735
779A-36R-2, 130–135	305.8	3,938	23		619
779A-36R-3, 45–50	306.5	9,554	45		852
779A-37R-1, 126–130	314.0	751	16		67
125-779B-1R-1, 135–140	1.4	8			0.0
779B-1R-3, 135–140	4.4	12			1.0
779B-1R-5, 135–140	7.4	6			0.6
779B-1R-6, 95–100	8.5	7			0.6

[a]Microliters of gas per liter of wet unconsolidated serpentine.
[b]Micromoles of methane per liter of interstitial water, assuming a porosity of 50%. Where values are absent, the gas was not detected.

Table 10. Composition of gas pockets in cores from Site 779, sampled through the core liner into an evacuated glass tube.

Core, section, interval (cm)		Depth (mbsf)	Methane (ppmv)	Ethane (ppmv)	Propane (ppmv)
125-779A-2R-5	38	7.48	10.9	0.8	nd
29R-2,	30	237.30	309,584	647.3	54.3
33R-1,	61	274.61	101,296	74.8	6.3
34R-1,101–105		284.73	154,405	203.8	15.5

nd = not detected.

PALEOMAGNETISM

Much of the sediment recovered from Hole 779A was disturbed during drilling. Lithologic Unit I is now a water-saturated slurry unsuitable for paleomagnetic work. Natural remanent magnetizations (NRM) of the material were measured to obtain a general idea of its magnetic properties. The archive halves of core sections were measured using the cryogenic magnetometer. NRM intensities vary, typically between 5 and 100 mA/m, but there is no apparent trend in these values downhole.

Material from Hole 779B proved much more useful for magnetostratigraphic studies, although the hole consisted of only a single core (an 8.7-m-thick interval of sediment). Whole-core NRM measurements were performed for Sections 125-779B-1R-1, 125-779B-2R, 125-779B-3R, 125-779B-5R, and 125-779B-6R. (Section 125-779B-1R-4 was not measured because it would not pass through the cryogenic magnetometer.) NRM intensities vary widely (between 10 and 400 mA/m), and there is a systematic decrease in these values downhole in the upper 2.5 m of the core (Fig. 22). In addition, each section was measured after alternating field (AF) demagnetization to 3, 5, 7, and 10 mT. The magnetostratigraphic results from Core 125-778-1R are presented in Figure 22. All sections carry dominantly reversed polarities, or have magnetizations that "trend" toward reverse at the 10-mT field value. Three short intervals (about 30 cm thick) with possibly normal polarities were also identified in Sections 125-779B-1R-5 and 125-779B-1R-6. The polarity recorded at these levels may be a depositional remanence, but may also represent viscous remanent magnetizations (VRM) from the present-day geomagnetic field that have not been completely demagnetized at the 10-mT step.

Discrete specimens were taken from the working halves of Sections 125-779B-1R-2, 125-779B-1R-3, 125-779B-1R-5, 125-779B-1R-6, and 125-779B-1R-7. For additional analysis, two specimens were taken from Section 125-779B-1R-1, and three specimens from Section 125-779B-1R-4. The specimens were AF demagnetized to 0, 3, 5, 8, 10, and 12 mT using the cryogenic magnetometer. Results from these specimens are summarized in Table 12. Specimens from Sections 125-779B-1R-1, 125-779B-1R-2, 125-779B-1R-3, 125-779B-1R-5, and 125-779B-1R-6 record a polarity similar to that of the adjacent interval in the section from which they were taken (Fig. 22). The three specimens from Section 125-779B-1R-4 are reversed, normal, and reversed downhole, respectively. The single discrete specimen from Section 125-779B-1R-7 is reversely magnetized.

Core 125-779B-1R exhibits a predominantly reversed polarity. Shipboard biostratigraphic studies ("Biostratigraphy" section, this chapter) have identified nannoplankton that have been assigned to the lower part of Okada and Bukry's (1980) Zone CN14a at these levels. This implies that the magnetization in the upper part of Hole 779B is a record of the middle part of the Matuyama Chron (based on magnetostratigraphic and biostratigraphic data presented by Berggren et al., 1985). This interval lies within the lower part of the Pleistocene.

Normal polarity levels within the lower part of the core (Section 125-779B-1R-6) may represent part of the Olduvai Event, or alternatively, could represent a VRM that was not completely demagnetized at the 10-mT step. The poor quality of data at these levels makes accurate correlation difficult.

Combined paleomagnetic and biostratigraphic data did enable us to date accurately the sediments overlying the serpentine "flows" on the southern flank of Conical Seamount. These data imply that the youngest possible age of these "flows" in this area must be earliest Pleistocene.

NRM measurements also were performed for the serpentine and serpentinite material beneath this thin cover of sediments in Hole 779A. Intensities were typically 50 to 250 mA/m. However, owing to the lack of biostratigraphic data and the highly altered and deformed state of the rock, we found it impossible to fit the data into any chronologic framework.

PHYSICAL PROPERTIES

Hole 779A

Physical properties at Site 779 were measured on whole-round core samples as well as discrete samples (Tables 13 to

Table 11. Composition of interstitial waters from cores at Site 779.

Sample number	Core section, interval (cm)	Volume (mL)	Squeeze T T (°C)	Depth (mbsf)	pH	Salinity (R.I., %)	Salinity (calc., %)	Chlorinity (mmol/kg)	Alkalinity (meq/kg)	Sulfate (mmol/kg)	Sodium (mmol/kg)	Potassium (mmol/kg)
Surface seawater (4 Mar. 1989)					8.10	35.5	34.85	542.6	2.386	27.98	464.8	10.05
1W-1	779A-2R-2, 145–150	18	2	4.08	7.50	36.0	34.81	543.9		27.77	464.3	10.12
1W-2	779A-5R-3, 46–56	30	2	33.11	9.08	33.8	33.68	529.4	1.361	22.46	483.3	10.52
1W-2	779A-13R-1, 140–150	20	6	108.05	11.62	32.2	34.06	523.1	7.482	19.19	545.5	10.56
1W-4	779A-18R-2, 7–17	4	2	156.52	11.76		35.48	525.5	11.677	25.56	575.3	9.89
[a]1W-41	779A-18R-2, 7–17	24	12	156.62	11.10	32.5	34.99	534.1	4.886	22.51	562.1	12.31
1W-5	779A-28R-2, 95–105	9	6	227.47	11.68	32.0	34.39	507.7	11.307	25.52	552.7	9.75
1W-6	779A-30R-1, 140–150	10	6	246.45	11.91	31.7	33.88	495.1	15.102	24.90	544.1	9.32
1W-7	779A-32R-2, 0–10	12	6	265.95	11.27	31.0	32.93	498.0	4.804	23.37	525.8	8.47
1W-8	779A-33R-1, 42–52	18	7	274.47	11.08	31.5	32.59	491.3	4.856	23.79	515.3	8.92
1W-9	779A-34R-1, 111–121	20	7	284.86	11.58	30.0	31.37	480.6	8.228	17.47	503.6	8.23
1W-10	779A-36R-2, 136–150	36	7	305.93	10.32	31.8	33.74	515.5	2.901	24.06	534.8	6.65
1W-11	779A-37R-1, 135–150	28	8	314.18	9.93	32.2	33.75	522.3	2.450	21.33	538.4	6.39
1W-1	779B-1R-1, 145–150	34	2	1.48	8.16	35.4	34.52	537.9	2.364	27.45	463.3	9.39
1W-2	779B-1R-3, 110–115	40	2	4.08	7.92	35.4	34.35	536.0	2.277	27.14	459.8	9.27
1W-3	779B-1R-5, 145–150	42	2	7.48	7.99	35.4	34.83	538.8	2.280	29.25	467.7	9.29
1W-4	779B-1R-6, 105–110	30	2	8.58	7.79	35.3	34.64	539.8	2.282	27.65	464.4	9.09

[a]Material trimmed from the exterior of the core sample prior to squeezing.
Values absent from table were not determined.

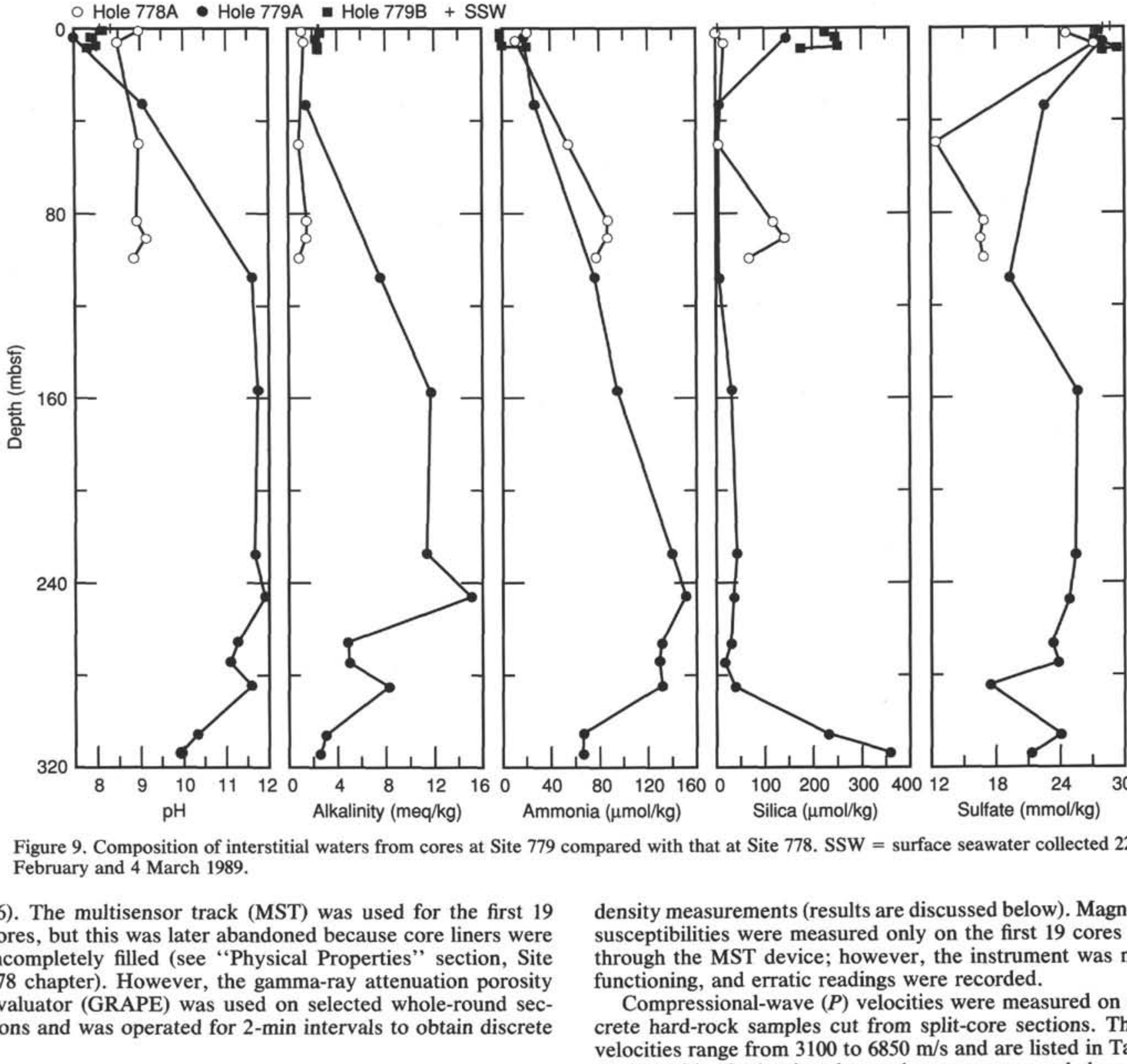

Figure 9. Composition of interstitial waters from cores at Site 779 compared with that at Site 778. SSW = surface seawater collected 22 February and 4 March 1989.

16). The multisensor track (MST) was used for the first 19 cores, but this was later abandoned because core liners were incompletely filled (see "Physical Properties" section, Site 778 chapter). However, the gamma-ray attenuation porosity evaluator (GRAPE) was used on selected whole-round sections and was operated for 2-min intervals to obtain discrete density measurements (results are discussed below). Magnetic susceptibilities were measured only on the first 19 cores run through the MST device; however, the instrument was malfunctioning, and erratic readings were recorded.

Compressional-wave (*P*) velocities were measured on discrete hard-rock samples cut from split-core sections. These velocities range from 3100 to 6850 m/s and are listed in Table 14. Velocities for hard-rock samples were measured along the core (vertically in the A direction) and, in some cases, perpendicular to the vertical (in the B direction, see Table 14). The velocities in both the A and B directions are shown in Figure 23. The average velocities for the hard-rock clasts are 4600 and 5000 m/s in the A and B directions, respectively. Velocities of soft sediment and serpentine samples were not measured because the samples tended to deform in the Hamilton Frame instrument.

Index properties were determined from the hard rocks sampled for velocity measurements. Index properties of soft sediment and serpentine samples also were measured using the same weight and volume determination scheme. The bulk-density measurements of these discrete samples are listed in Table 13. Plots of bulk densities from all specimens are shown in Figure 24.

In addition, bulk densities of hard rocks were measured in selected whole-round sections by the 2-min GRAPE method discussed above. These values range from 1.95 to 3.09 g/cm^3 (Fig. 25) and average 2.55 g/cm^3.

Table 11 (continued).

Calcium (mmol/kg)	Magnesium (mmol/kg)	Bromide (mmol/kg)	Silica (μmol/kg)	Ammonia (μmol/kg)	Phosphate (μmol/kg)
10.17	52.89	0.85	5	<5	
9.76	53.45	0.87	146	18	
9.32	31.62	0.78	5	27	0.27
6.41	0.029	0.85	5	76	
1.55			30	95	
4.55	0.213	1.10	19	45	
3.81	0.002	0.98	41	140	<0.10
3.29	0.005	0.96	35	152	
7.37	0.316	0.92	30	131	
9.69	0.038	0.96	15	129	
5.96	0.022	0.94	37	132	
6.31	6.218	0.78	230	66	<0.10
6.74	4.540	0.79	361	66	<0.10
8.92	52.33	0.73	230	<5	0.82
9.63	52.10	0.98	250	<5	1.15
9.60	51.73	0.88	255	<5	0.93
9.84	52.12	0.90	176	22	0.71

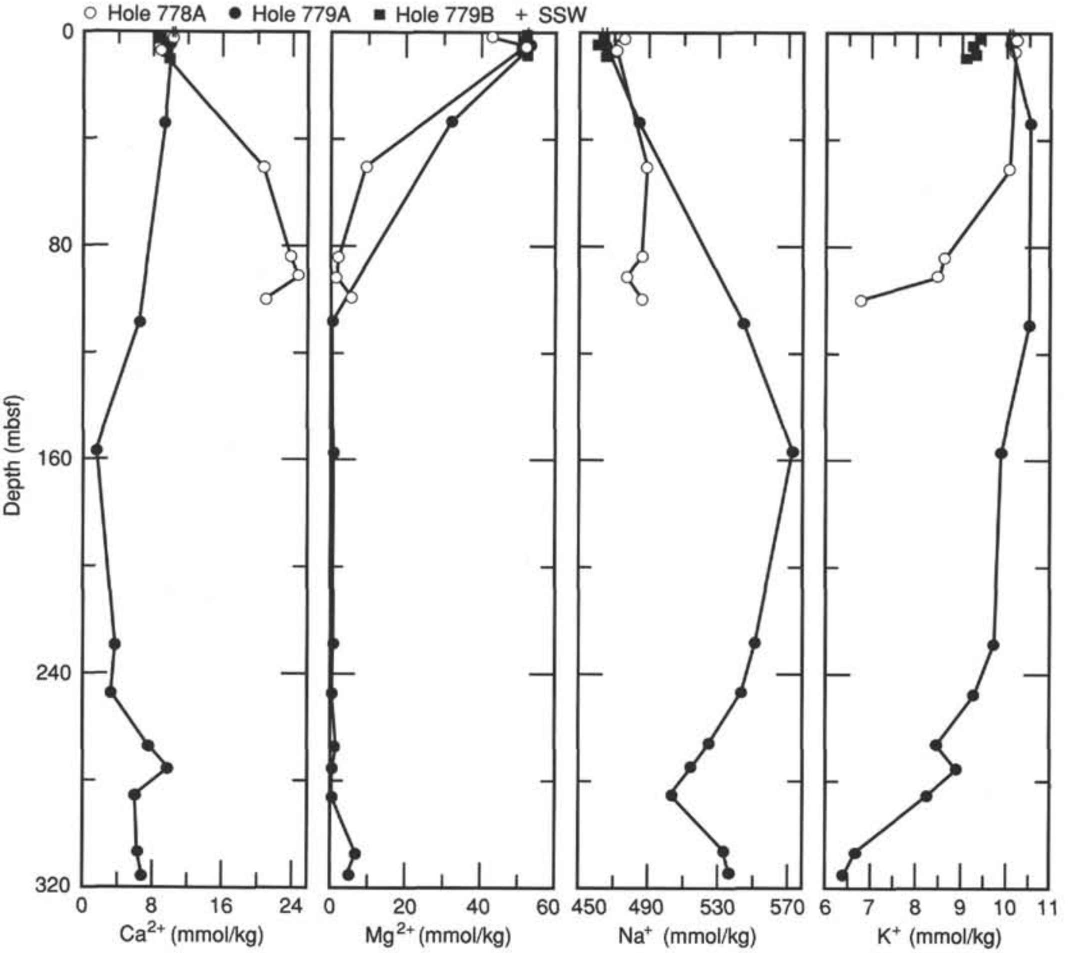

Figure 10. Composition of interstitial waters from cores at Site 779 compared with that at Site 778. SSW = surface seawater collected 22 February and 4 March 1989.

Thermal conductivities were measured on both soft whole-round core samples and on hard, slabbed core subsamples. Thermal conductivity values for soft-core samples ranged from 0.852 to 2.342 W/mK and averaged 1.807 W/mK for 15 measurements (Table 14). The values for the soft-core samples are plotted in Figure 26. Thermal conductivity values for hard-rock samples ranged from 1.397 to 3.233 W/mK and averaged 2.148 W/mK for 24 measurements (Table 14). The hard-rock measurements are plotted in Figure 27.

Hole 779B

Only one core was recovered from Hole 779B. Three bulk-density measurements were performed, which are listed in Table 15. Four conductivity measurements were also run for this core, the results of which are shown in Figure 28. Resistivity and formation-factor values are listed in Table 14.

SUMMARY AND CONCLUSIONS

Site 779 (19°30.75′N, 146°41.75′E; water depth, 3947.2 mbsl) is a second flank site on Conical Seamount situated halfway up the southeast flank, about 3.5 km northeast of Site 778. Two holes were drilled: Hole 779A (which reached 319.2 mbsf) and Hole 779B (which was a single 9-m core aimed at recovering the uppermost sediment). Recovery at Hole 779A averaged 22.9% (Table 1, Fig. 29).

Three major lithologic units were recovered at Site 779:

1. Unit I (0–10.6 mbsf in Hole 779A and 0–9 mbsf in Hole 779B): Holocene(?) to lower Pleistocene unconsolidated sediments and unconsolidated serpentine flows comprising clay, silt-sized serpentine, and lithic fragments in a matrix of sand- and silt-sized serpentine.
2. Unit II: lower Pleistocene(?) to lower Pliocene(?) or upper Miocene(?).

Subunit IIA (10.6–216.2 mbsf): sheared serpentine containing clasts of variably serpentinized harzburgite and subordinate variably serpentinized dunite and metabasalt in a serpentine matrix.

Subunit IIB (216.2–303.0 mbsf): sheared serpentine containing clasts of serpentinized harzburgite with subordinate serpentinized dunite, gabbro and metabasalt in a serpentine matrix with intercalations of detrital serpentine sediments.

3. Unit III (303.0–317.2 mbsf): serpentine microbreccia with convolute layering.

Dating of Hole 779A is based on biostratigraphic data that give Quaternary ages for Unit I (early Pleistocene for its base), and late Miocene(?) to early Pliocene(?) ages for the top of Subunit IIB (this section also contained reworked Oligocene nannofossils). Dating of Hole 779B is based on combined biostratigraphic and magnetostratigraphic evidence: the former gives Pleistocene ages, the latter suggests that the upper part of the hole may record the middle part of the Matuyama Chron (just below the Pliocene/Pleistocene boundary).

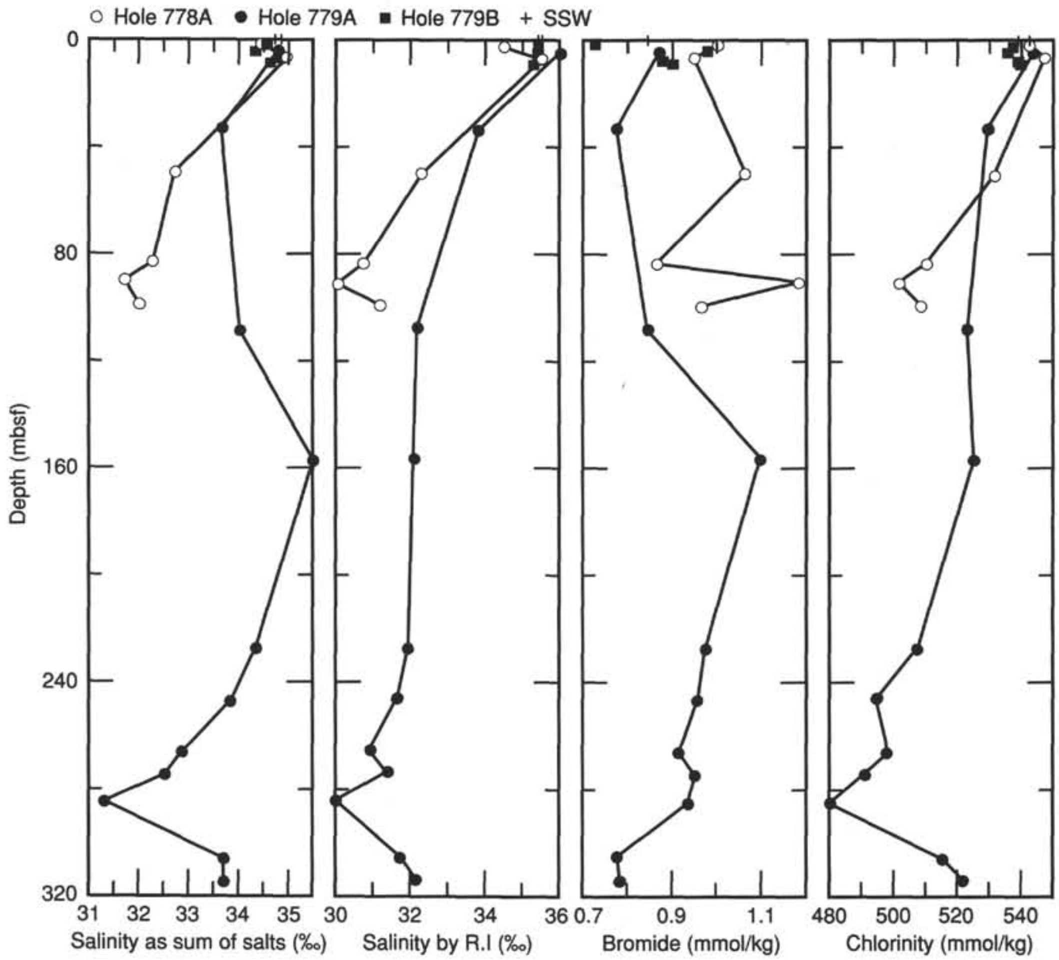

Figure 11. Composition of interstitial waters from cores at Site 779 compared with that at Site 778. SSW = surface seawater collected 22 February and 4 March 1989.

The serpentine-rich material in Subunit IIB contains recrystallized carbonate, kerogen(?), and filamentous opaque mineral aggregates that may be bacterial remnants. The presence of kerogen would indicate a primary sedimentary origin for this material, an interpretation supported by the presence of horizontal bedding and nannofossils within the same unit.

Hard-rock lithologies are mostly of two types: serpentinized, tectonized ultramafic rocks and subordinate metabasic rocks. The ultramafic rocks are mostly harzburgite and subordinate dunite, with primary mineralogies similar to those of Hole 778A. The degree of serpentinization varies, but indicates an overall decrease downhole. Serpentine veins are common and indicate a polystage filling history. Mafic clasts are predominantly metabasalt and metagabbro of primary mineralogy dominated by plagioclase and clinopyroxene and (in basalts) glass; one microgabbro is about 3 m thick in the cored section. Common metamorphic minerals are clay minerals, chlorite, pumpellyite, and rarely, albite and sphene.

Structures indicate a complex history of deformation comparable to that described in Hole 778A. In addition, detailed studies of Subunit IIA have shown that no consistent interrelationships exist between ultramafic clasts, suggesting that this unit at least represents a chaotic formation. The presence and orientations of brittle-ductile conjugate faults in the clasts of Subunit IIB indicate extension about a vertical axis, and the deformation of the matrix is consistent with gentle flowage under an applied load.

Analyses of interstitial pore-water samples at Site 779 show major variations from 0 to 100 mbsf: pH increases to a maximum of 11.9; alkalinity increases five-fold; ammonia and sodium show significant but smaller increases; calcium decreases by 80%; both salinity and chlorinity decrease by 10%; and potassium and sulfate show small decreases. Magnesium is totally depleted below 80 mbsf. These results confirm the presence of a fluid other than seawater, possibly from the subducting plate, as proposed for Site 778. However, the fluids contrast in detail with those from Site 778, particularly in calcium concentration, which decreased at this site yet doubled over the same interval in waters from Site 778, thus indicating considerable lateral variation in interstitial water composition within the flank materials of the seamount. Hydrocarbons increased dramatically with depth in Hole 779A, with methane, ethane, and propane present in most samples. A maximum of 30% methane was analyzed from one gas pocket sampled through the core liner.

The principal results of Site 779 can be summarized as follows:

1. The site provides further evidence for the depleted nature of the mantle wedge beneath Conical Seamount.
2. Flowage of unconsolidated serpentine coupled with sedimentary processes are important in the construction of Conical Seamount.

3. Hydrocarbons are an important component of the fluids associated with the seamount.

4. The serpentinite source region has experienced medium-grade metamorphism.

5. Water derived from the subducted slab might be an important source of fluids involved in the serpentinization of Mariana forearc materials.

REFERENCES

Barron, J. A., 1985. Late Eocene to Holocene diatom biostratigraphy of the equatorial Pacific Ocean, Deep Sea Drilling Project Leg 85. *In* Mayer, L., Theyer, F., et al., *Init. Repts. DSDP*, 85: Washington, (U.S. Govt. Printing Office), 413–456.

Berger, W. H., 1970. Planktonic foraminifera: selective solution and the lysocline. *Mar. Geol.*, 8:1–11.

Berggren, W. A., Kent, D. V., Flynn, J. J., and Van Couvering, J., 1985. Cenozoic geochronology. *Geol. Soc. Am. Bull.*, 96:1407–1418.

Berner, R. A., and Honjo, S., 1981. Pelagic sedimentation of aragonite: its geochemical significance. *Science*, 211:940–942.

Fryer, P., Ambos, E. L., and Hussong, D. M., 1985. Origin and emplacement of Mariana forearc seamounts. *Geology*, 13:774–777.

Haggerty, J. A., 1987. Petrology and geochemistry of Neogene sedimentary rocks from Mariana forearc seamounts: implications for emplacement of the seamounts. *In* Keating, B. H., Fryer, P., Batiza, R., and Boehlert, G. W. (Eds.), *Seamounts, Islands, and Atolls*, Geophys. Monogr. Ser. 43: Washington (Am. Geophys. Union), 175–185.

Hussong, D. M., and Fryer, P., 1985. Forearc tectonics in the northern Marianas arc. *In* Nasu, N., Kobayashi, K., Uyeda, S., Kushiro, I., and Kagami, H. (Eds.), *Formation of Active Ocean Margins*: Tokyo (Terrapub), 273–290.

Li, Y.-H., Takahashi, T., and Broecker, W. S., 1969. Degree of saturation of calcium carbonate in the oceans. *J. Geophys. Res.*, 75:5507–5525.

Okada, H., and Bukry, D., 1980. Supplementary modification and introduction of code numbers to the low-latitude coccolith biostratigraphic zonation (Bukry, 1973, 1975). *Marine Micropaleontology*, 5:321–325.

Pearce, J. A., and Cann, J. R., 1973. Tectonic setting of basic volcanic rocks determined using trace element analysis. *Earth Planet. Sci. Lett.*, 19:290–300.

Pearce, J. A., and Wanming, D., 1988. The ophiolites of the Tibetan Geotraverse, Lhasa to Golmud (1985) and Lhasa to Kathmandu (1986). *Phil. Trans. R. Soc. London A.*, 327:215–238.

Ms 125A-108

NOTE: All core description forms ("barrel sheets") and core photographs have been printed on coated paper and bound as Section 4, near the back of the book, beginning on page 383.

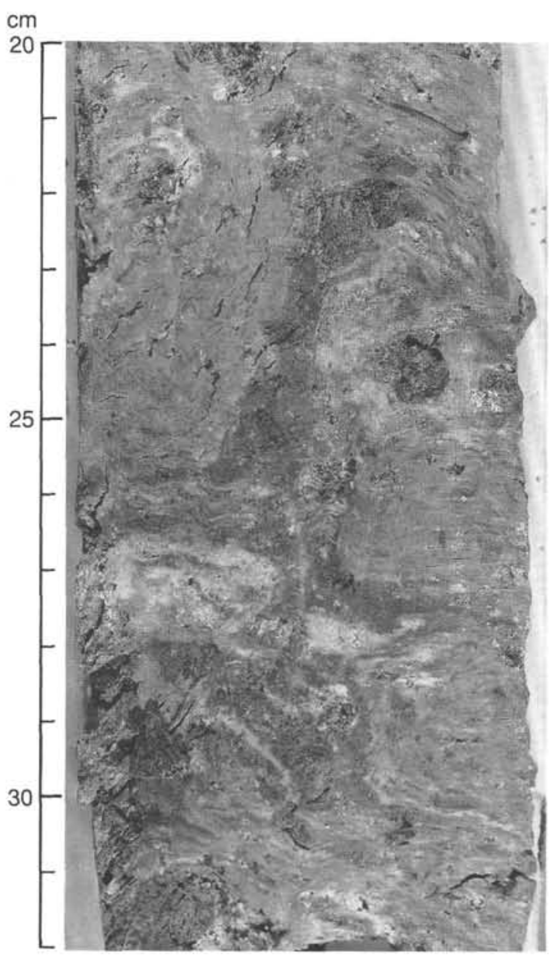

Figure 12. Interval 125-779A-7R-1, 20–32 cm, showing successive convolute folds affecting the serpentine sediments, flows, and microbreccias.

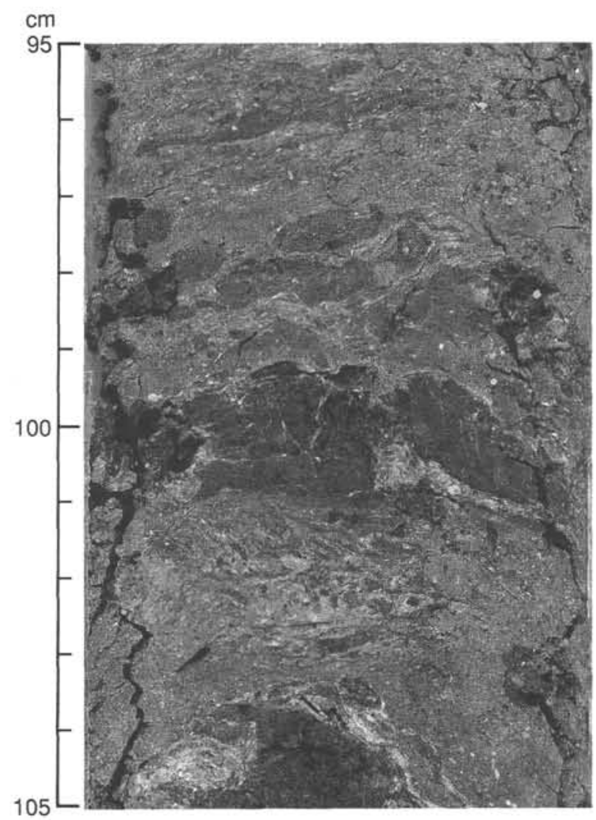

Figure 13. Interval 125-779A-13R-1, 95–105 cm. Primary layering and late foliation and scaly clay cleavage developed within the serpentine siltstones and microbreccias.

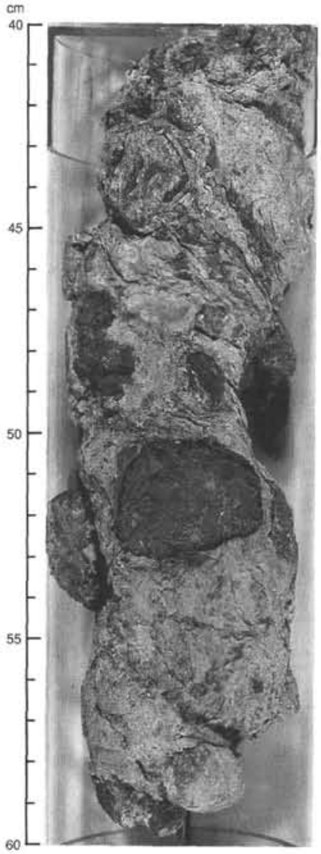

Figure 14. Interval 125-779A-20R-1, 40–60 cm, showing helicoidal cleavage and asymmetric shape of clasts.

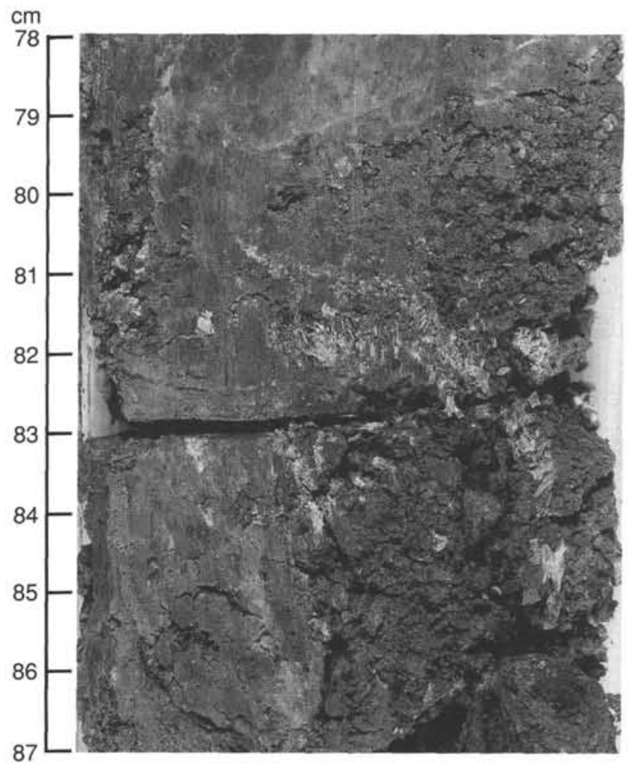

Figure 15. Detailed view of Interval 125-779A-18R-2, 78–87 cm. Vertical chrysotile fibers developed in a vein opened in the soft serpentine sediments. The vein is deformed along the edge of the core, probably as a result of drilling disturbance.

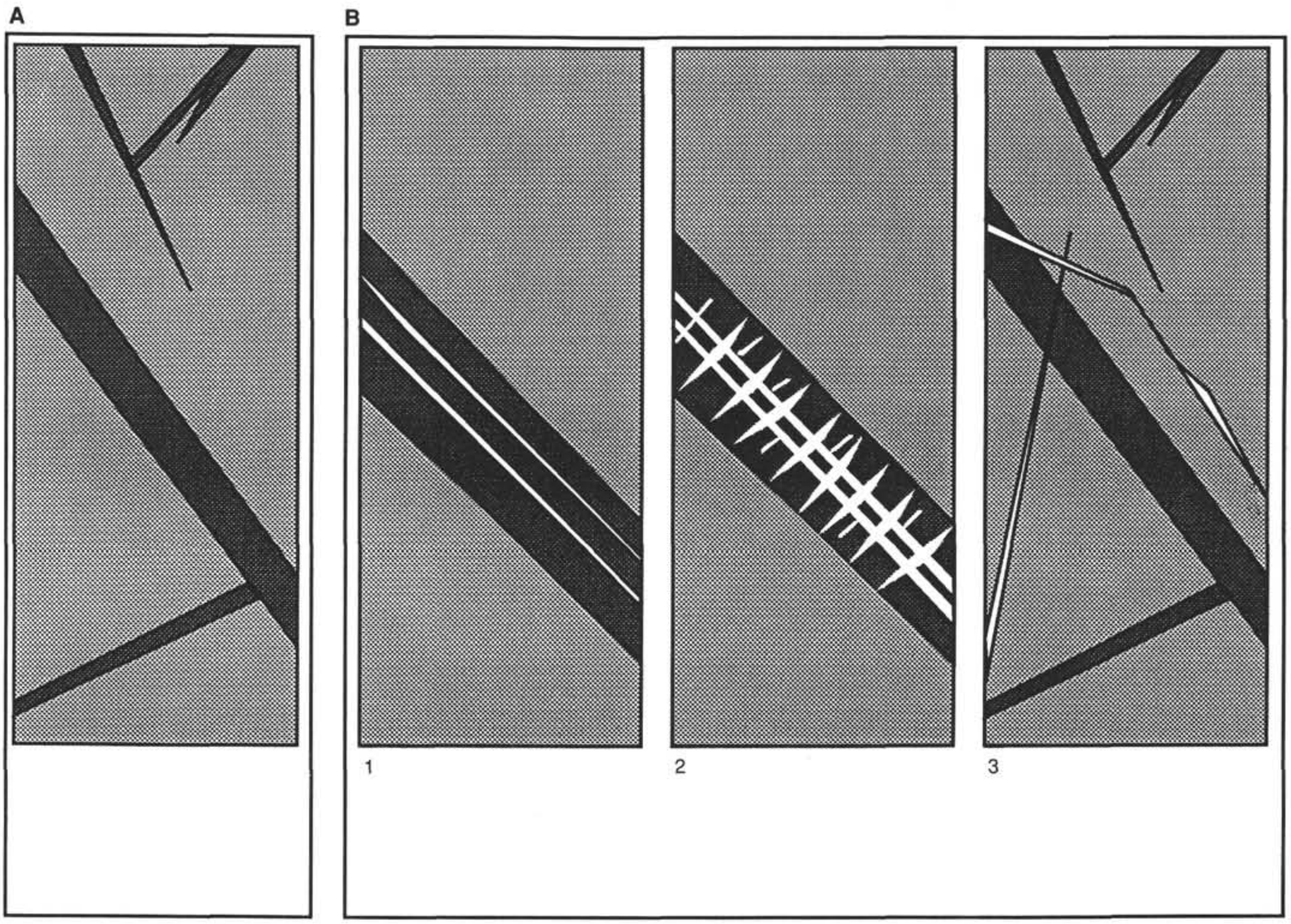

Figure 16. The main types of serpentine veins crosscutting the ultramafic rocks in lithologic Unit II. A. Early antigorite veins. B. Late chrysotile veins (1, 2, and 3 refer to the three subtype veins described in text).

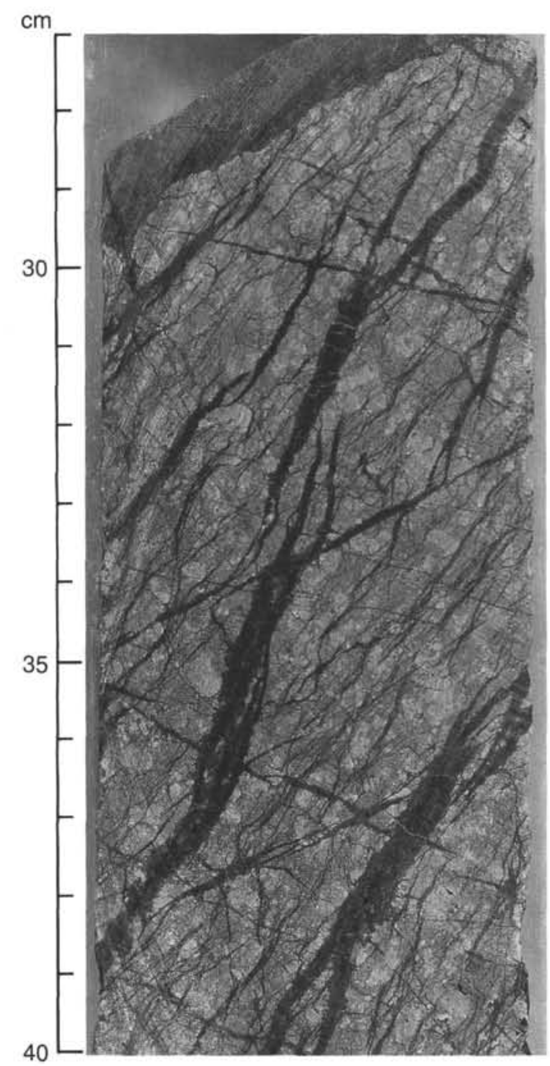

Figure 17. Antigorite veining in Interval 125-779A-17R-2, 27–40 cm. Anastomosing veining defines centimeter-size lenses of serpentinized peridotites. Notice that the uppermost centimeter of the piece corresponds to a major vein.

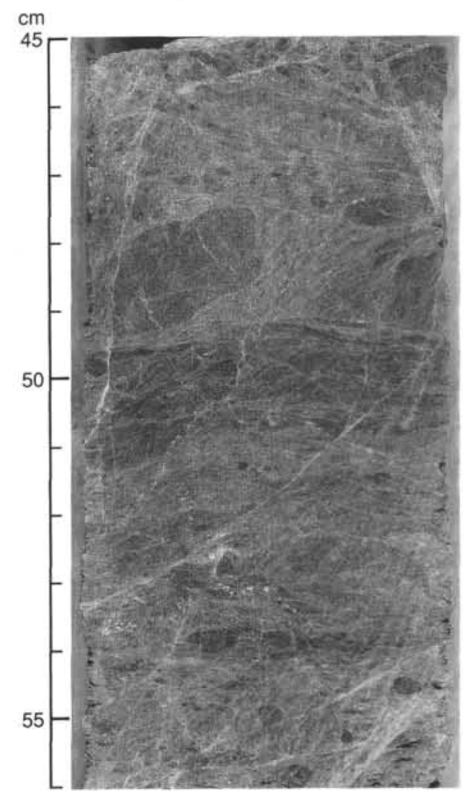

Figure 18. Interval 125-779A-31R-1, 45–56 cm. Cataclasis in a serpentine tectonic breccia.

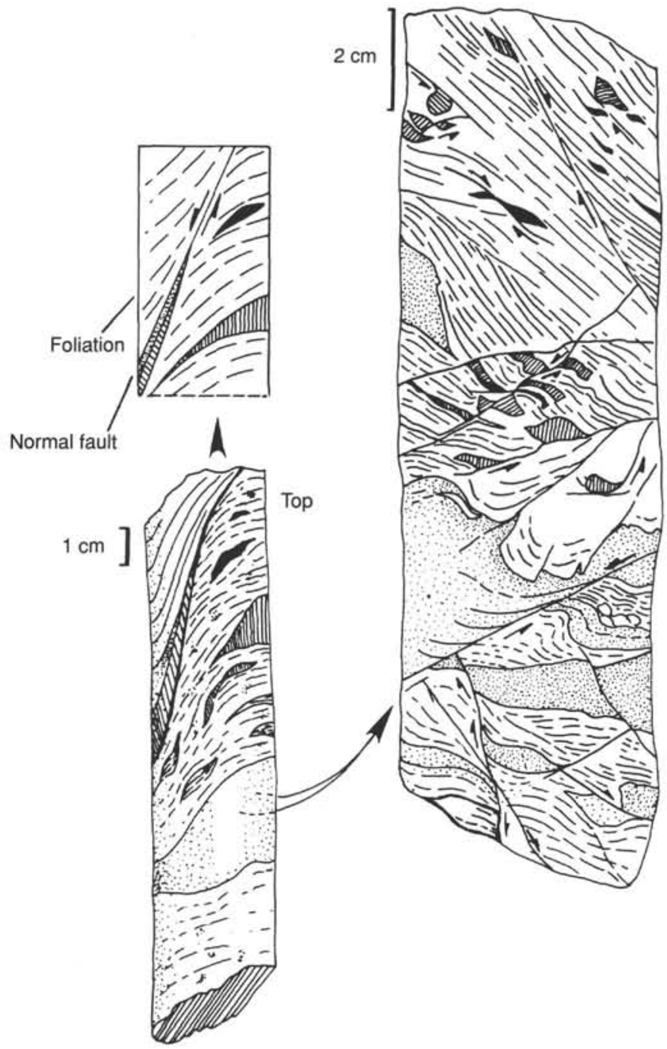

Figure 19. Interpretation of the tectonic fabric observed in Interval 125-779A-30R-2, 34–52 cm.

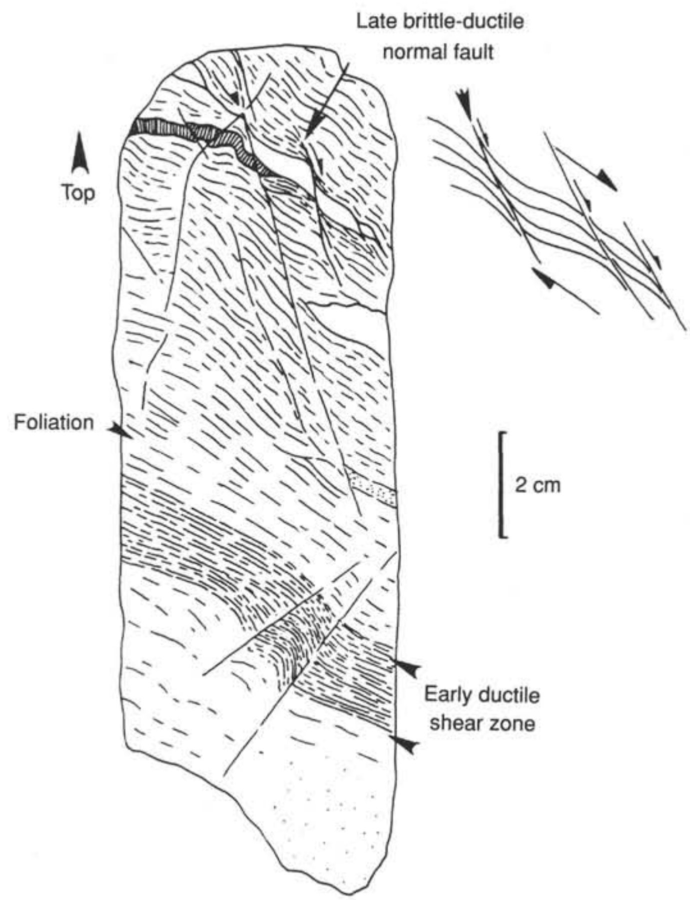

Figure 20. Interpretation of the tectonic fabric observed in Interval 125-779A-31R-2, 80–93 cm.

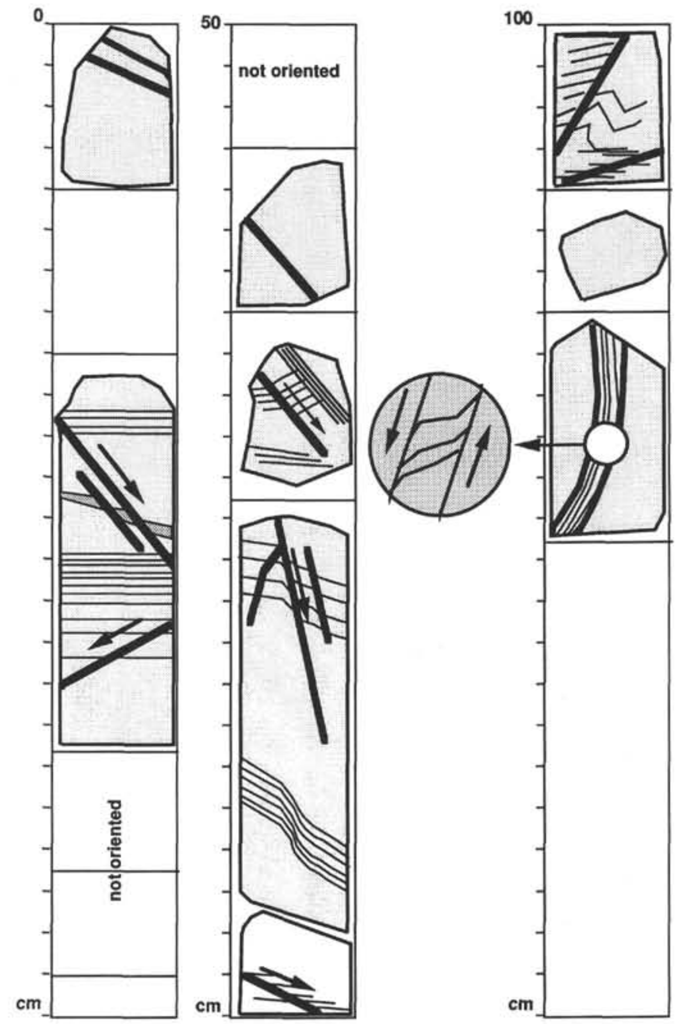

Figure 21. Summary of the main results related to the tectonic fabric analysis of Section 125-779A-31R-2 (sheared metamicrogabbros). Thick lines represent late brittle faults with a sense of movement indicated. Thin lines parallel the early foliation. The core was split so that the apparent dip of the major faults would correspond to the true dip.

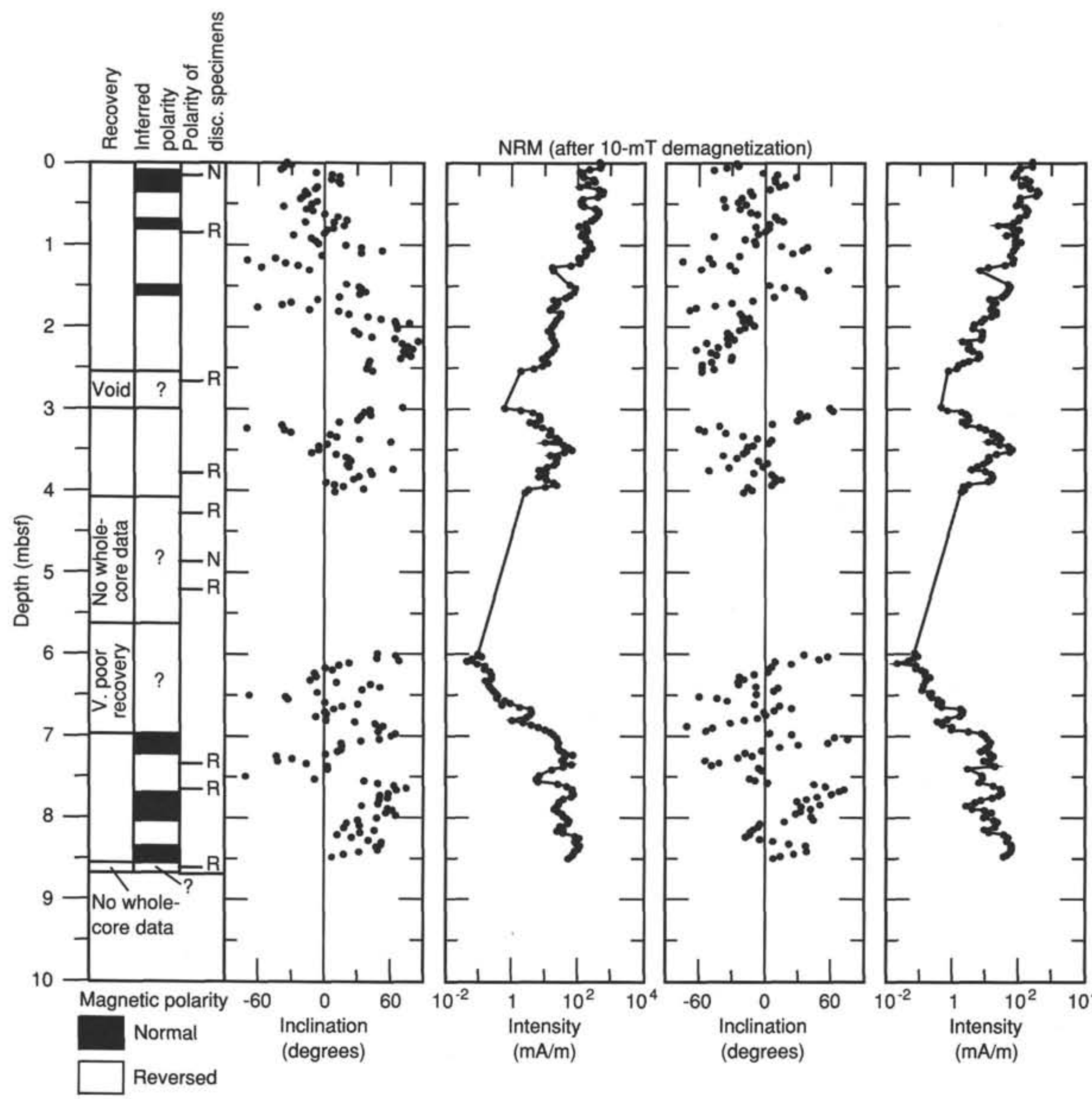

Figure 22. Magnetostratigraphic results from Core 125-779B-1R. Note (A) the downhole decrease in magnetic intensity between 0 and 2.5 m and (B) the shift toward predominantly negative magnetic inclination angles at the 10-mT demagnetization step in the upper 4 m of core.

Table 12. Paleomagnetic data for discrete specimens taken from Core 125-779B-1R.

		NRM			RM at 12 mT			
Section	Top (cm)	DEC (degrees)	INC (degrees)	INT (mA/m)	DEC (degrees)	INC (degrees)	INT (mA/m)	Polarity
125-779B-1R-1	14	9.1	71.5	23.77	11.1	55.1	13.33	N
1R-1	86	147.6	25.7	3.74	172.2	−56.1	3.27	R
1R-2	63	194.9	−2.8	4.70	279.6	−11.3	14.71	R
1R-3	76	263.7	15.3	26.94	156.4	−50.3	6.79	R
1R-4	20	31.9	−34.8	3.91	257.4	−37.4	4.83	R
1R-4	76	353.4	−5.9	4.98	317.4	23.4	1.81	N
1R-4	108	141.0	−17.0	17.80	156.0	−25.6	16.97	R
1R-5	125	84.0	35.6	16.05	141.4	−62.5	5.15	R
1R-6	9	18.4	50.5	4.61	277.3	−20.0	3.24	R
1R-CC	6	353.0	−27.5	387.67	7.5	−18.8	192.12	R

NRM = Natural remanent magnetization; DEC = Declination; INC = Inclination; INT = Intensity of magnetization; RM = remanent magnetization. (Note the rather large increase in intensity for the specimen from Section 125-779B-1R-2). N = normal; R = reversed.

Table 13. Index properties of sediments from Holes 779A and 779B.

Core, section interval (cm)	Depth (mbsf)	Bulk density (g/cm^3)	grain density (g/cm^3)	Porosity (%)	Water content (%)	Void ratio
125-779A-2R-2, 85–86	3.45	1.82	5.69	82.9	48.2	0.83
2R-3, 136–137	5.46	1.67	2.66	60.5	38.5	0.61
2R-4, 86–87	6.46	1.35	2.7	80.6	63.5	0.66
2R-5, 36–37	7.46	1.58	2.66	66.3	44.7	0.66
3R-CC, 17–20	10.77	2.67	2.67	0.3	0.1	0
4R-1, 27–29	20.37	2.29	2.29	0	0	0
4R-1, 58–59	20.68	1.95	2.66	43.6	23.8	0.44
5R-2, 34–37	31.39	2.83	2.83	0	0	0
5R-3, 34–35	32.89	1.88	2.65	47.8	27.1	0.48
6R-1, 18–20	39.38	2.99	3.01	0.9	0.3	0.01
6R-1, 46–47	39.56	1.99	2.62	39.3	20.9	0.39
8R-1, 25–27	58.75	2.39	2.54	9.6	4.3	0.1
8R-1, 45–49	58.95	2.7	2.7	0	0	0
9R-1, 33–35	68.43	1.89	2.35	349	19.6	0.35
9R-2, 52–54	70.05	2.64	2.64	0	0	0
10R-2, 70–73	79.63	2.74	2.74	0.5	0.2	0.01
13R-1, 91–92	107.51	1.86	2.86	54.6	31.2	0.55
14R-1, 76–78	116.96	2.87	2.87	0	0	0
14R-2, 60–62	118.3	2.94	2.94	0.1	0.1	0
16R-3, 48–50	138.98	2.86	2.88	1	0.4	0.01
17R-1, 81–83	146.01	2.99	3	0.3	0.1	0
17R-2, 30–32	147	2.96	2.96	0.1	0	0
17R-3, 30–32	148.42	2.76	2.76	0	0	0
18R-1, 64–67	155.54	1.94	2.64	43.6	23.9	0.44
18R-2, 27–31	156.67	2.17	2.71	32.1	15.8	0.32
18R-3, 13–4	157.94	2.31	2.99	34.6	15.9	0.35
19R-2, 97–99	161.87	3.04	3.04	0	0	0
22R-1, 58–60	170.68	2.65	2.65	0	0	0
22R-1, 63–65	170.73	2.73	2.73	0	0	0
22R-2, 18–20	171.78	2.86	2.86	0.1	0.1	0
22R-3, 55–67	173.65	2.82	2.82	0	0	0
24R-1, 36–38	187.56	2.86	2.86	0	0	0
25R-1, 85–87	197.65	2.65	2.65	0	0	0
26R-2, 50–52	207.94	2.71	2.71	0	0	0
26R-3, 101–103	209.56	2.57	2.58	1.2	0.5	0.01
27R-1, 57–59	216.77	1.9	2.59	44.3	24.8	0.44
28R-2, 58–59	227.05	1.98	2.67	41.8	22.4	0.42
28R-3, 26–28	228.23	2.64	2.64	0	0	0
29R-2, 33–35	236.23	1.86	2.71	50.3	28.7	0.5
30R-1, 48–49	245.48	1.81	2.52	47.2	27.6	0.47
30R-2, 87–89	247.17	2.45	2.63	11.1	4.8	0.11
31R-1, 26–28	254.96	2.47	2.64	10.7	4.6	0.11
31R-CC, 39–41	258.64	3.2	3.2	0	0	0
32R-1, 123–125	265.63	2.01	2.76	43.4	23	0.43
32R-2, 17–19	266.07	2.11	2.61	31.4	15.8	0.31
33R-2, 46–48	274.98	2.92	2.92	0.1	0	0
34R-1, 36–38	284.06	2.59	2.59	0	0	0
35R-1, 13–7	293.37	2.62	2.62	0	0	0
35R-1, 108–109	294.38	2.99	3	0.5	0.2	0.01
36R-1, 46–47	303.46	2.18	2.62	27.4	13.3	0.20
36R-1, 70–71	305.2	2.02	2.82	44.4	23.3	0.44
37R-1, 49–50	313.19	1.96	2.62	41.1	22.2	0.41
37R-2, 13–4	314.24	2.15	2.62	30	14.8	0.3

Table 14. Physical properties of sediments from Holes 779A and 779B.

Core section, interval (cm)	Depth (mbsf)	Thermal conductivity (W/mK)	Resistivity (ohms)	Formation factor	"A" Velocity (km/s)	"B" Velocity (km/s)
125-779A-1R-1, 47–51	0.50	1.004	23.4	2.73		
2R-1, 37	1.47	1.577				
2R-1, 127–131	2.39		21.4	2.50		
2R-3, 37	4.47	1.399				
4R-1, 27–29	20.37				3.10	
5R-2, 32–35	31.37				5.08	
5R-2, 40–43	31.45				6.85	
5R-3, 45	33.00	1.522				
6R-1, 18–20	39.28					4.18
6R-1, 39	39.49	1.876				
7R-1, 93	49.43	2.291				
8R-1, 25–27	58.75					3.64
8R-1, 33	58.83	2.403				
8R-1, 45–49	58.95				4.94	
9R-2, 35	69.88	2.227				
9R-2, 52–54	70.05					3.04
10R-2, 70–73	79.63					5.44
13R-1, 51	107.11	1.930				
13R-1, 74–78	107.36		76.0	8.87		
13R-1, 100–104	107.62		115.0	13.42		
13R-2, 11	108.21	2.062				
13R-2, 92–94	110.00				3.36	3.38
14R-1, 76–78	116.96				3.36	
16R-3, 48–50	138.93				5.27	5.15
17R-1, 81	146.01	2.257				
17R-2, 30	147.00	2.708				
17R-3, 30	148.42	1.889				
17R-4, 20	149.82	2.149				
18R-2, 37–41	156.76	2.298	184.0	21.48		
18R-2, 75–79	157.17		63.0	7.35		
19R-2, 97–99	161.87				5.15	5.27
20R-1, 12	169.22	1.483				
20R-1, 73	169.83	2.180				
22R-1, 58–60	170.68				4.22	3.91
22R-1, 63–65	170.75	3.200			4.56	4.88
22R-2, 18–20	171.78				6.06	6.23
22R-3, 55–57	173.65				4.91	5.86
24R-1, 36–38	187.56				4.23	
25R-1, 81	197.61	2.330				
25-1, 85–87	197.65				5.29	
26R-3, 94	209.49	2.140				
26R-2, 0	207.44	2.000				
26R-2, 50–52	207.94				5.01	
26R-3, 101–103	209.56				4.96	
28R-3, 26–28	228.23					4.31
28R-3, 116	229.13	1.574				
29R-2, 28–32	237.30		37.3	4.35		
29R-2, 147–149	237.35	1.571				3.18
30R-1, 139	238.00	2.022				
30R-2, 84	247.14	2.285				
31R-1, 18	254.88	2.279				
31R-1, 26–28	254.96				3.57	
31R-1, 124	255.94	1.709				
31R-2, 94	257.14	3.233				
31R-2, 103–105	257.23				5.34	4.79
31R-3, 27	257.90	3.014				
31R-CC, 39–41	258.64				4.77	4.88
32R-1, 67–71	265.09		78.3	9.14		
32R-1, 117–121	265.60	2.086	55.2	6.44		
32R-2, 51–55	266.43		82.4	9.62		
32R-2, 81–85	266.73		58.0	6.77		
32R-3, 1	267.41	1.775				
33R-2, 46–48	274.98				4.59	3.85
33R-2, 73	275.25	1.579				
33R-3, 8	275.50	1.397				
34R-1, 32	284.02	1.745				
34R-1, 36–38	284.06				5.12	5.24
35R-1, 13–7	293.30	2.677			5.23	5.65
35R-1, 108–109	294.31	1.937			5.52	5.66
36R-1, 58	303.58	1.749				
36R-1, 43	304.63	2.092				
36R-2, 13–17	304.93		50.6	5.91		
36R-2, 56–60	305.08		60.6	7.07		
36R-2, 76–80	305.28		47.6	5.56		
36R-2, 110–114	305.62		62.3	7.27		
37R-1, 35–39	313.07		44.0	5.14		
37R-1, 100–104	313.70	2.342	106.0	12.37		
37R-2, 10	314.30	2.027				
125-779B-1H-1, 13–7	0.09		22.5	2.63		
1H-1, 60–64	0.62		22.4	2.61		
1H-1, 126–130	1.28		18.5	2.16		
1H-2, 15–19	1.67		19.5	2.28		
1H-2, 83–87	2.35		20.5	2.39		
1H-2, 98–102	2.50		31.4	3.67		

Table 15. Physical properties of sediments from Hole 779B.

Core section, interval (cm)	Depth (mbsf)	Bulk density	Gram density (g/cm^3)	Porosity (%)	Water content (%)	Void ratio
125-779B-1H-2, 43–45	1.93	1.74	2.6	54.5	33.2	0.54
1H-5, 91–93	6.91	1.81	2.79	55.7	32.7	0.56
1H-6, 48–50	7.98	1.55	2.67	68.3	46.9	0.68

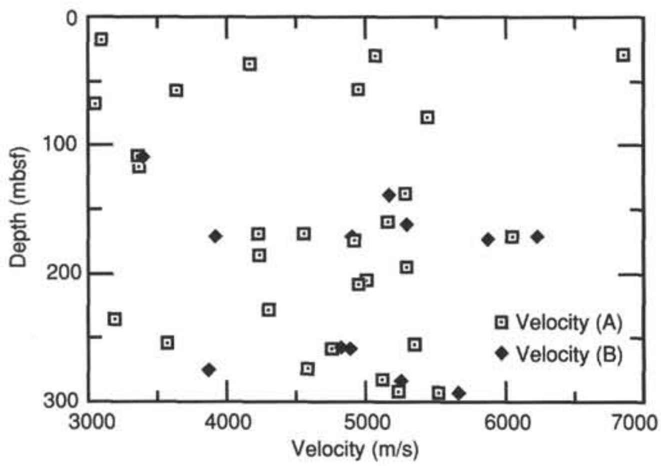

Figure 23. Velocity of subsamples vs. depth in Hole 779A. Velocities measured in the vertical direction along the core are labeled A and velocities measured in the horizontal direction perpendicular to the core are labled B. Note the scatter in the data.

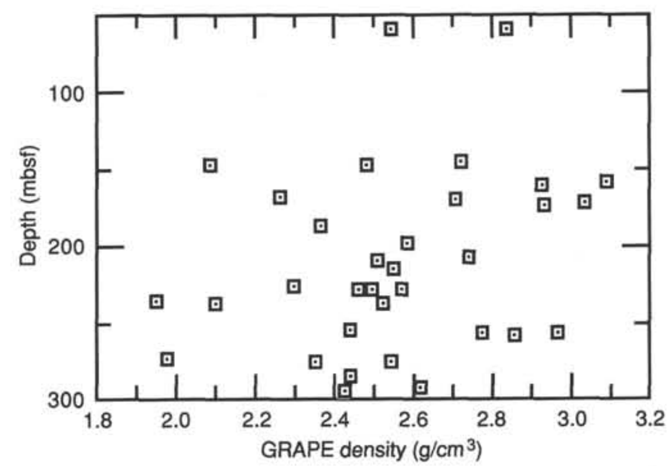

Figure 25. Densities from 2-min GRAPE analysis of whole-round, hard-rock core samples vs. depth in Hole 779A. Note the scatter in the data.

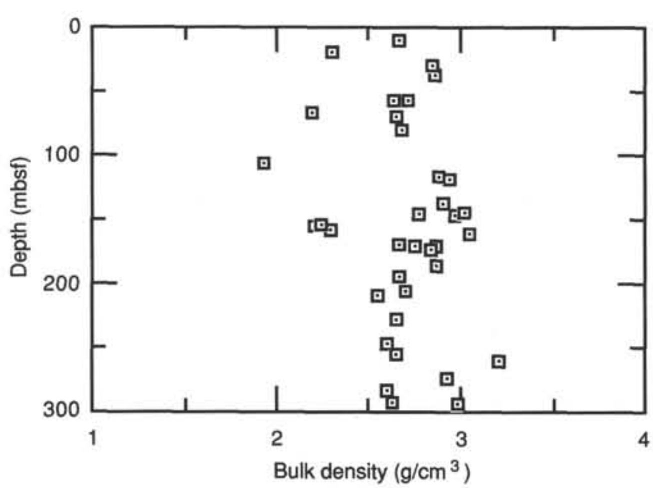

Figure 24. Bulk densities of hard-rock subsamples vs. depth in Hole 779A.

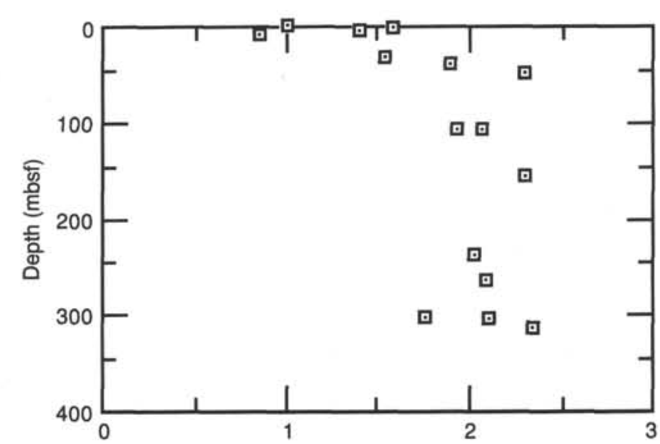

Figure 26. Thermal conductivity of soft, whole-round core samples vs. depth in Hole 779A. Measurements were performed using a needle probe that penetrated the core liner into the core. Conductivity increases slightly in the upper part of the hole and is then nearly constant to the bottom of the hole.

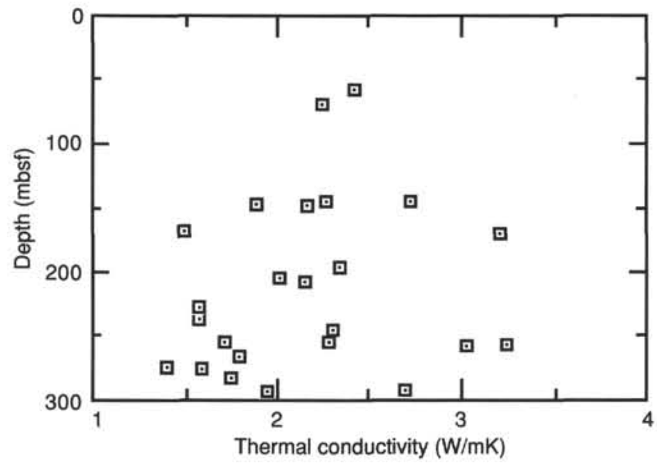

Figure 27. Thermal conductivity of hard-rock subsamples vs. depth in Hole 779A. Note the scatter in the data.

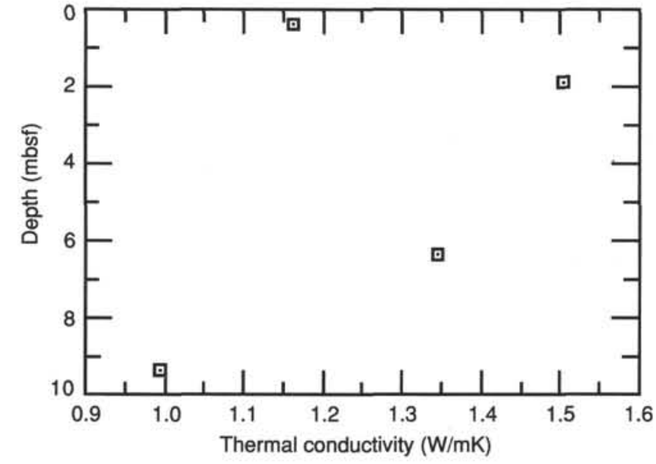

Figure 28. Conductivity measurements (in W/mK) for soft core samples (through the core liner) from Hole 779B.

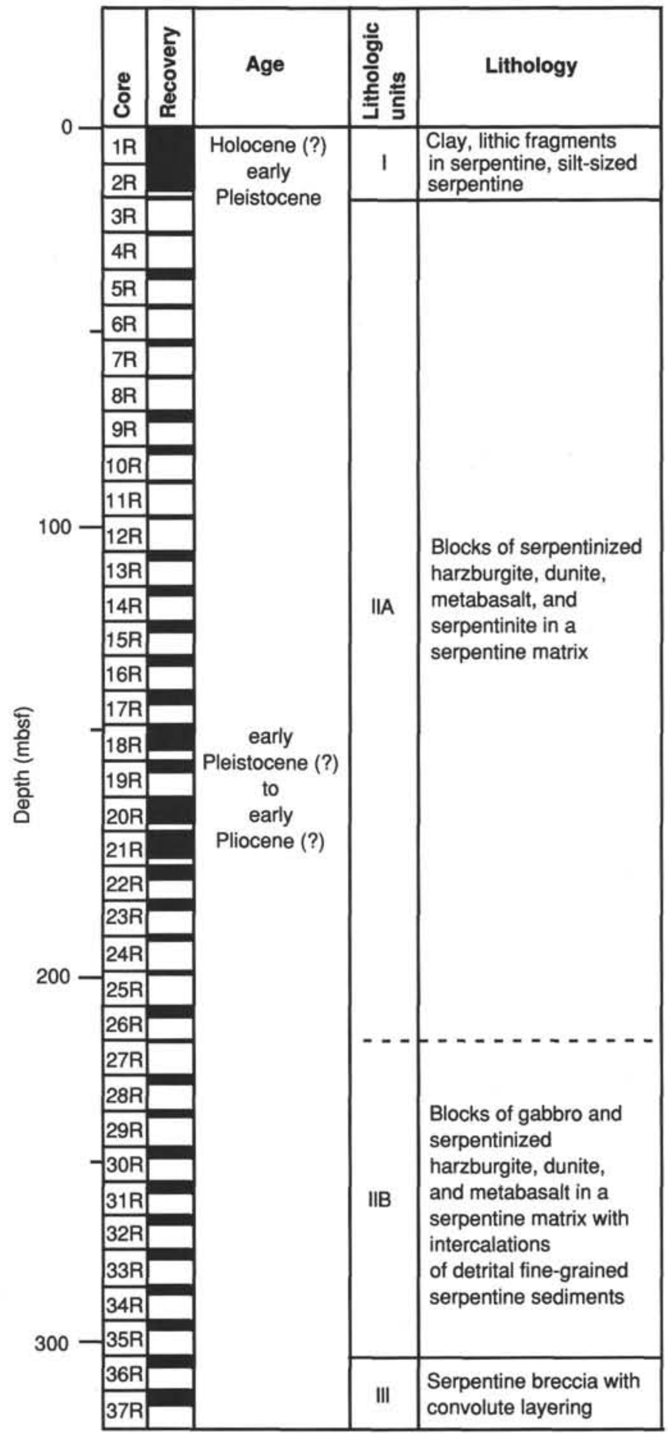

Figure 29. Core recovery and lithologic summary, Hole 779A.